AN ABSTRACT OF THE THESIS OF

Michael D. Long for the degree of Master of Science in Materials Science presented on April 28, 2006.

Title: The Creep and Microstructure of Copper.

Abstract approved: Signature redacted for privacy.

Michael E. Kassner

Creep experiments were conducted on copper polycrystals deformed within the five-power-law regime. The dislocation structure of copper, which has not been extensively characterized in the past, consists of less-well-defined subgrain walls of relatively low misorientation, typically between 0.1 and 0.3 deg, with a Frank network of dislocations within the subgrains. The subgrains were probed from one boundary to another in copper using convergent-beam electron diffraction (CBED). This allowed a determination of any changes in the lattice parameter, which would indicate the presence of any internal stresses. Earlier investigations by others suggested that internal stresses may be high in the vicinity of the "hard" subgrain boundaries in both loaded and unloaded specimens, based on a variety of techniques including X-ray diffraction (XRD), stress-dip tests, as well as some preliminary CBED. It was determined in this work that the lattice parameter was unchanged at the equilibrium or stress-free value within the interior of the subgrains and along (within a one-beam diameter) the subgrain boundaries.

THE CREEP AND MICROSTRUCTURE OF COPPER.

by

Michael D. Long

A THESIS

Submitted to

Oregon State University

in partial fulfillment of
the requirements for the
degree of

Master of Science

Presented April 28, 2006

Commencement June 2007

Master of Science thesis of Michael D. Long presented on April 28, 2006.

APPROVED:

Signature redacted for privacy.

Major Professor, representing Materials Science

Signature redacted for privacy.

Head of the Materials Science Program

Signature redacted for privacy.

Dean of the Graduate School

I understand that my thesis will become part of the permanent collection of Oregon State University libraries. My signature below authorizes release of my thesis to any reader upon request.

Signature redacted for privacy.

Michael D. Long, Author

ACKNOWLEDGEMENTS

The author wishes to acknowledge support from the U.S. Department of Energy Basic Sciences under contract DE-FG03-99ER45768. The author is also grateful for the assistance in submicrostructural characterization by Mark Wall of Lawrence Livermore National Laboratories and Dr. M.T. Perez-Prado currently of CENIM, CSIC Madrid, Spain. The authors would also like to acknowledge the assistance of Albany Research Center for assistance with annealing.

TABLE OF CONTENTS

LIST OF FIGURES

TABLE OF FIGURES (CONTINUED)

LIST OF TABLES

LIST OF APPENDICES

LIST OF APPENDIX FIGURES

NOMENCLATURE

A_{HD}	Harper-Dorn equation constant
b	Burgers vector
C_1-C_2	constants
d_o	original sample diameter
D_c	diffusion constant (pre-exponential)
D_o	diffusion coefficient
D_{sd}	lattice self-diffusion coefficient
E	Young's modulus
F_t	weight on Satec elevator tray
g	average grain size
G	shear modulus
I_o	x-ray diffraction intensity
k	Boltzmann's constant
l_o	original sample length
n	steady-state creep exponent
Q_c	activation energy for creep
Q_p	activation energy for pipe diffusion
Q_{sd}	activation energy for self-diffusion
t	time
T	temperature
T_m	melting temperature
v_t	transducer voltage
v_{to}	transducer set voltage
α	Taylor equation constant
ε_p	plastic strain
$\dot{\varepsilon}$	strain rate
$\dot{\varepsilon}_{ss}$	steady-state strain rate
λ	average subgrain size
λ_{ss}	steady-state subgrain size
ν	Poisson's ration
θ	misorientation angle across high angle boundaries
θ_λ	misorientation angle across low angle boundaries
θ_x	x-ray diffraction angle
ρ	dislocation density (subgrain/cell interior)
ρ_{ss}	steady-state dislocation density (subgrain/cell interior)
σ_{ss}	steady-state stress

The Creep and Microstructure of Copper.

1. INTRODUCTION

Copper, from the Latin cuprum, is believed to have been mined for over 5,000 years and is used in many applications from an alloying element to extensive use as a conducting material. Despite its extensive and historical significance, copper has seen limited use a structural element mostly because of its poor mechanical properties. This lack of mechanical strength has provided little incentive to characterize the submicrostructural properties of copper, most specifically the dislocation densities and subgrain features. Understandably, the creep behavior and microstructure of more common structural alloys, such as iron, titanium, and aluminum have been extensively investigated. Previous creep studies of Cu have, almost without exception, had intentions of pure research. One interesting exception dealt with the electrical resistance of power transmission lines that grew in length, due to creep deformation, over their lifespan in tropical India.

Another reason copper properties have not been characterized is due to the difficulty associated with testing copper at elevated temperatures. There are three particularly pervasive problems that preclude more extensive investigations of copper properties. These include oxidation, activation energy changes, and dynamic recrystallization.

Five-power law creep behaviors of materials, including copper, are well characterized. However, what is not well understood is the fundamental deformation mechanisms on a submicroscopic level. Several theories have been developed to help explain the nature of these creep studies, but their scope has been limited by the ability to characterize the microstructure.

There are two areas of interest involved with this study. The first is the characterization of the subgrain microstructure of copper under five-power law creep conditions. The dislocation density is well characterized for other metals. Some studies

of other fcc metals, most specifically aluminum, indicate that the dislocations form well defined sub-grains, and yet other works [1] indicate that subgrains do not form in copper. Insights into these creep microstructural properties are provided in this analysis.

The second area if interest also extends beyond copper. One important concept in the metallurgical community is that of internal (or back) stresses. Many have adopted the concept of internal stresses or bowing grain boundaries to explain the nature of strength of metals during deformation. However, the theories are not yet been proven experimentally. By performing an in depth analysis of the microstructure perhaps some light can be shed on the nature of long range internal stresses.

The purpose of this investigation was to perform Scanning Electron Microscopy and Convergent Bema Electron Diffraction analysis of five power law creep copper specimens. Data from this will be compared to previous literature values followed by a discussion of their implications.

2. LITERATURE REVIEW

2.1 CREEP REGIMES

Creep of a metal is most easily defined as the time dependent deformation of a given material under fixed stress. The term "creep" likely arose because materials will plastically strain under a moderate and constant stress, in comparison to the yield stress, at a conventional strain rate. Figure 1 shows what is generally known as a strain vs. time curve illustrating the three creep regimes. Stage I, or primary creep, is the region in which the sample is loaded and the strain rate decreases to a steady state value. This changing of strain rates is due to the hardening of the metal due to increasing dislocation densities, resulting in decreasing strain rates. The strain rate decreases to the steady state value shown in the Stage II regime.

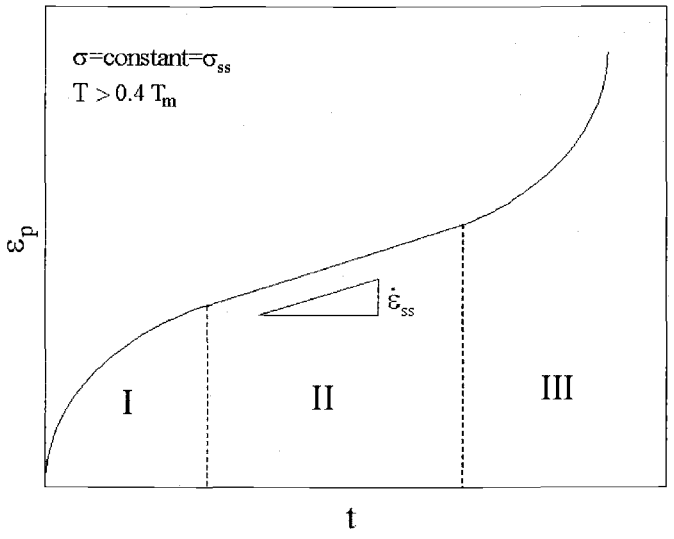

Figure 1. Creep Regimes.

Stage II creep is of most interest to the scientific community. It is within this regime that the lowest steady state strain rate is achieved, as defined by Eq. 1. It is also during Stage I and Stage II that dislocations are created and the relevant sub-microstructure is formed, including subgrains and dislocation densities within the interior of subgrains. If deformation is allowed to continue the material cavitates. This region of increasing strain rate is known as State III, or ternary creep, and eventually leads to fracture.

$$\dot{\varepsilon} = \frac{\delta}{\delta t}\varepsilon_p \tag{1}$$

2.2 CREEP EQUATIONS

It is well understood that n-power-law creep systems are complex and require a broader understanding of the deformation of metals. This includes an understanding of the relationships between stress, strain rate, dislocation density, subgrain size, and thermal effects, as well as others. An equation has been developed to phenomenologically characterize five-power law creep systems: [2]

$$C_1 \frac{\dot{\varepsilon}_{ss} kT}{D_c Gb} = \left(\frac{\sigma_{ss}}{G}\right)^n \tag{2}$$

Where k is Boltzmann's constant, T is the testing temperature, D_c is the lattice diffusivity, G is the shear modulus and b is the Burgers vector. The diffusivity factor in Eq. 2 is defined by the following:

$$D_c = D_o \exp\left(\frac{-Q_c}{kT}\right) \tag{3}$$

For this report, a commonly accepted value for D_o high purity Cu of 0.2 cm^2/s was used. [3]

There is a large source of controversy surrounding the activation energy term, Q_c. It has been verified that for most pure metals above 0.5 T_m the lattice self-diffusion energy, Q_{sd}, is the activation energy for creep, but several works on copper show this not

to be the case. Early works on Cu suggest a value comparable to that of the vacancy diffusion for temperatures greater than 0.7 T_m, [4,5,6] approximately 197,066,400 Joules/mol, and a value for lower temperatures closer to that expected for pipe diffusion Q_p, approximately 125,520,000 Joules/mol.

As illustrated in Figure 2 [7] there is a region in which the activation energy undergoes a transition from Q_p to Q_{sd}. The controversy involves how the activation energy changes between these two regimes. Barrett and Sherby[4], Gilbert and Munson [8]and Feltham and Meakin[9] describe a transition that almost appears like a step function. Pahutova et. al[10] and Retima and Cornet[11] believe that this shift of Q_c is due to some dependency on stress.

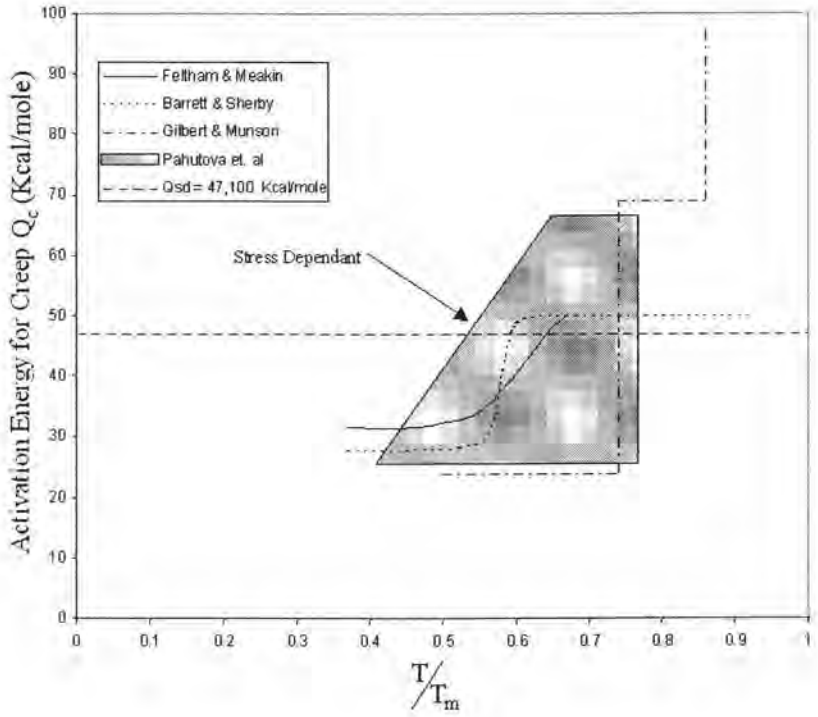

Figure 2. Activation Energy Plot. (based on [7])

Raj and Langdon [7] describe three points of disagreement with how each of the previously mentioned works describe this shift in activation energy. The first refers the reported values of Q_c. Barrett and Sherby and Feltham and Meakin reported a step change in the activation energy from about 0.6 Q_{sd} to 1.0 Q_{sd} at approximately $0.7T_m$. While others, including Pahutova and Gilbert and Munson, report activation energies from near 0.5 Q_{sd} to significantly greater than Q_{sd}, at $T>0.7T_m$. The second discrepancy involves how Pahutova et. al and Retima and Cornet describe a phenomenon that appears to show the changes in Q_c be stress dependent. Furthermore, Raj and Langdon show a linear dependence of Q_c with stress. Thirdly, there seems to be very little agreement between the various investigations as to where the activation energy shift occurs.

Usually, the activation energy for metals and alloys over the five-power law regime corresponds to the lattice self-diffusion energy with a decrease in the activation energy for creep during power law breakdown (PLB) at roughly 0.5-0.6 T_m. It has often been suggested that, within PLB, the decrease in Q_c corresponds to a switch to dislocation pipe diffusion Q_p; with the rate controlling mechanism for creep remaining dislocation climb. In the case for Cu, the same arguments made by Barrett and Sherby [4,5] have been applied except that the transition to climb control by vacancy diffusion via dislocation pipes occurs at relatively high temperatures well-within five-power law behaviors at 0.7 T_m. Raj and Langdon [7] performed an extensive investigation of the activation energy properties in both the literature and their own investigation and concluded that there is a more gradual transition of Q_c, than reported by Barrett and Sherby, between the stresses of $\sigma/G=3x10^{-4}$ to $\sigma/G=2x10^{-3}$.

This controversy surrounding Q_c is complex and as of yet is unresolved. It is necessary to use a constant value for the analysis of this study. It was decided to use the lattice self-diffusion energy regardless of the temperature or stress above 0.6 T_m. Correcting for this assumption in equations 2 and 3,

$$C_1 \frac{\dot{\varepsilon}_{ss} kT}{D_{sd} Gb} = \left(\frac{\sigma_{ss}}{G} \right)^n \tag{4}$$

And

$$D_{sd} = D_o \exp\left(\frac{-Q_{sd}}{kT} \right) \tag{5}$$

The shear modulus is a compensation term for an apparent increase in creep strength with the modulus, and allows a comparison to other materials. [12] Also, modulus compensation allows for greater phenomenological accuracy. While either the choice of Young's or shear modulus is phenomenologically reasonable, the choice of shear modulus is more common. This term can be easily compensated for temperature effects with a polynomial curve fit to well established data. Koster[13], in Figure 3, provides a modulus temperature dependence, data was confirmed by Barrett[4] with an oscillating beam deflection experiment.

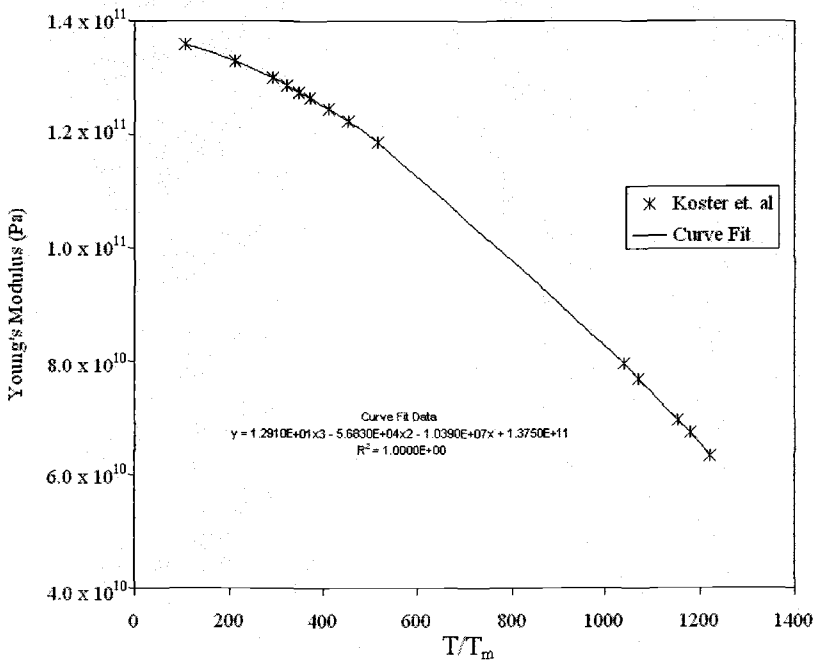

Figure 3. Elastic Modulus vs. Temperature Data.

It can be seen that with a third order polynomial equation a high confidence (R^2=0.9999) curve fit can be developed to approximate the Young's modulus of copper. This equation for the modulus data is as follows,

$$G(T) = 1.2910 \cdot 10^{3} T^{3} + 5.6830 \cdot 10^{4} T^{2} + 1.0390 \cdot 10^{7} T + 1.3750 \cdot 10^{11} \quad (6)$$

The conversion between Young's Modulus and the shear modulus utilized:

$$G(T) = \frac{E(T)}{2(1+\nu)} \quad (7)$$

A value for Poisson's ratio, ν, of 0.34 was used. [14]

2.3 NORMALIZED DATA

Using Eq. 4 a normalized plot, shown in Figure 4, of Cu steady-state creep from the previous works is illustrated. [4,5,7,10,15,16,17] Several assumptions were made in selecting data for this plot. Studies were chosen with data within 0.4 T_m to 0.8 T_m, where T_m is the absolute melting temperature. It is obvious that five-power law is observed with this data set, with PLB beginning at $\sigma/G \sim 10^{-3}$.

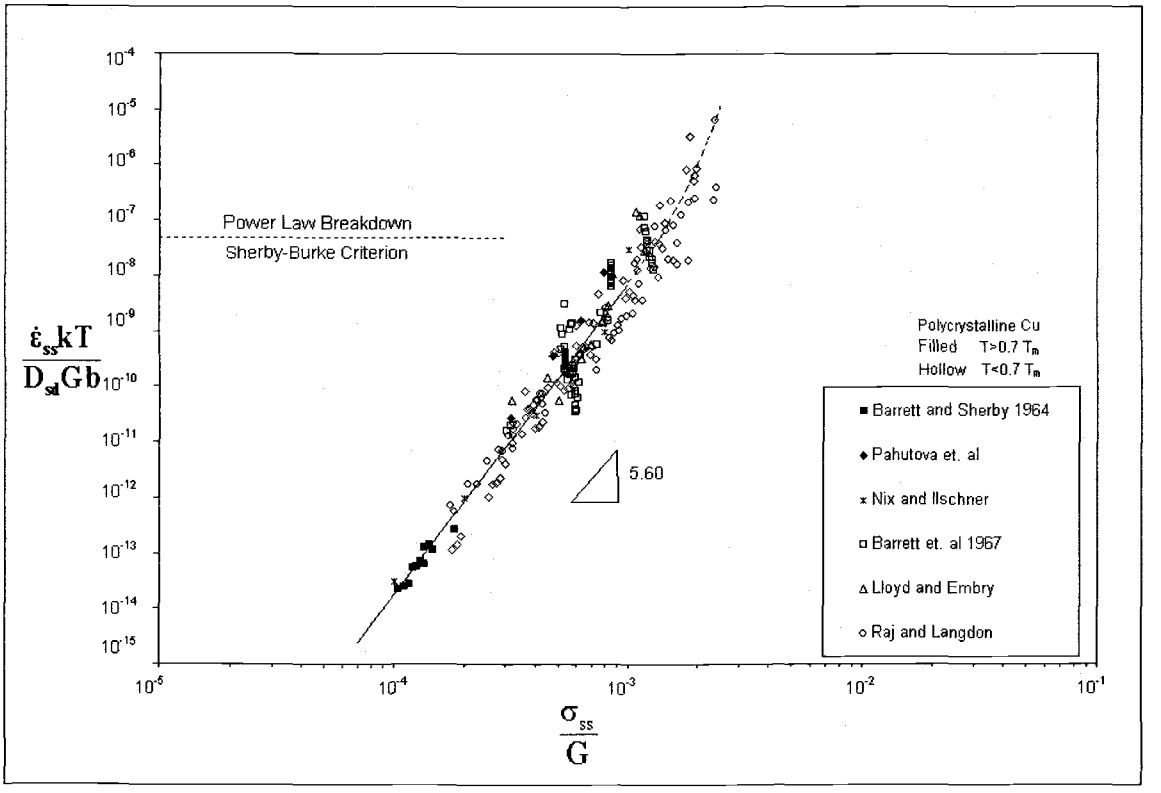

Figure 4. Normalized Steady State Creep Data of Cu

Each point on the plot describes a normalized condition where the abscissa is a normalized stress point, but the value in the ordinate can vary depending on the strain rate and temperature. To add in the complexity, even the abcissa is not absolute value of stress because of stress temperature compensation.

As will be discussed later a perspective must be developed relating the relation ship between the variables of five-power law creep. This perspective must take into account the relative relationship of temperature effects, stress, and strain rate, as well as the implications on the microstructure.

2.4 OTHER CREEP MECHANISMS

While this study is an investigation of the five-power creep properties of copper it is appropriate to mention other creep mechanisms. Some investigations have shown that under conditions of high temperature and low stresses power-law creep is still controlling (with lower stress exponents.) These other mechanisms are called diffusional creep, Harper-Dorn creep, or power-law breakdown (PLB).

Diffusional creep is observed at low stresses and high temperatures. Originally thought to only occur at temperatures greater than $0.9T_{m,}$ studies have suggested it to occur as low as $0.7\ T_m$. Diffusional creep mechanisms differ from five-power creep mechanisms in that the former does not involve dislocation glide or climb. In five-power creep dislocations glide through the lattice, but at a rate controlled by dislocation climb. In diffusional creep mass transport occurring of vacancies either through the grain or along the grain boundary, by Nabarro-Herring and Coble respectively

Nabarro-Herring creep involves movement of vacancies through the grain at high temperatures and low stresses. As seen in Figure 5, excess vacancies are created at the grain boundaries, lying normal to the tensile axis. These vacancies are then transported to the grain boundaries parallel to the tensile stress axis.

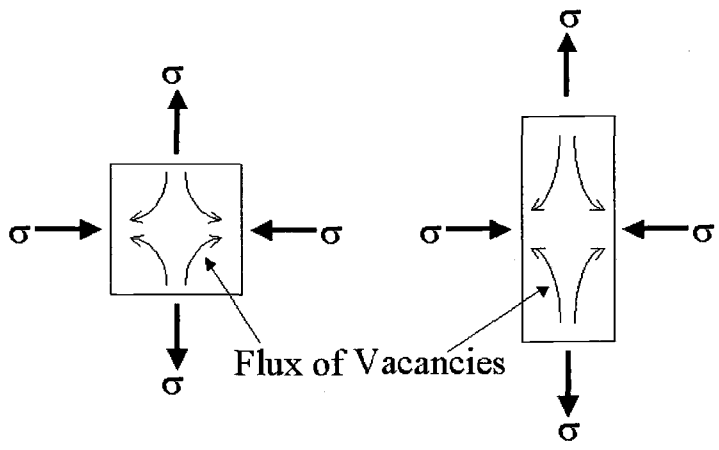

Figure 5. Diffusional Creep Model.

This mass transport of vacancies allows grains to elongate without dislocation movement. The strain rate for Nabarro-Herring creep is:

$$\dot{\varepsilon}_{ss} = \frac{D_{sd}\sigma b^3}{kTg^2} \tag{8}$$

Where g is the grain size.

The second form of diffusional creep is Coble creep. Proposed in 1953, Coble creep is based on the implication that for temperatures between $0.7T_m$ and T_m grain boundary diffusion rates exceed that for lattice self-diffusion. Reportedly observed in Cu [18], the strain rate is:

$$\dot{\varepsilon}_{ss} = \frac{\alpha^3 D_{gd}\sigma b^4}{kTg^3} \tag{9}$$

Both in Nabarro-Herring and Coble creep there appears to be a lower limit of stress below which measurable strain rates, or creep, is no longer observed. This appears to be temperature dependent and related to the stacking fault energy. Because vacancy

diffusion is the controlling mechanism, and the concentration of vacancies cannot exceed the steady state (equilibrium) value there is no primary creep regime.

Another form of creep that occurs at high temperature and low stresses is Harper-Dorn creep. This mechanism was proposed in 1957 as an explanation for low sress-exponent aluminum creep that showed rates some 1400 times larger than those predicted by diffusional creep models. These high temperature large-grained samples also showed a classical Stage I, or primary creep regime and a linear dependence (though not strictly so) between strain rate and applied stress.

There appears to be two limiting factors for this form of creep: grain size and stress. Studies have shown that under a limiting grain size, g_t, Nabarro-Herring creep occurs, but over this grain size Harper-Dorn creep dominates. It is interesting to note that within these larger grain sizes, above g_t, Harper-Dorn strain rates appear to be grain size independent. The strain rate for Harper-Dorn creep has been shown to follow:

$$\dot{\varepsilon}_{ss} = A_{HD}\left(\frac{D_{sd}Gb}{kT}\right)\left(\frac{\sigma_{ss}}{G}\right)^{1} \qquad (10)$$

Regardless of T or g, as the applied stress exceeds a critical value, σ_p, the strain rates begin to increase giving way to five power-law creep.

This dashed line shown in Figure 4, of increasing slope, denotes the region called power-law breakdown. PLB is still not well understood, but it is thought to be a transition from climb to glide controlled plasticity.[19] Previous works show that for many pure metals PLB to occur at $\sigma/G=1.23\text{x}10^{-3}$, which corresponds to the data plotted. [20,21] Sherby and Burke also describe this with a value of $\dot{\varepsilon} / D \cong 10^{13}$ m-2. [21] A good correlation can be observed between the Sherby-Burke criterion and the onset of PLB in the reported data.

2.5 GENERAL MICROSTRUCTURE

The microstructure of five-power law creep samples is quite interesting and can help in developing theories about strength of materials that encompass not only the five-power regime, but other stress, strain, and temperature regimes.

As a molten metal cools, different regions begin to crystallize in various orientations. Rather than these regions forcing themselves to reorient, high-energy grain boundaries are created. Each of these grains contain a relatively homogenous structure and crystal orientation. These high-energy grain boundaries are typically misoriented between 10°-62°, or θ for cubic materials. During plastic deformation as dislocations are created and move through the grains they attempt to reach a lowest energy state. This is a consequence of the residual tensile, compressive, and shear strain effects of a dislocation in a crystal, shown in Figure 6a. One method for reducing the elastic strain energy is for the dislocations to coalesce to an arrangement, as shown in Figure 6b, for edge dislocations.

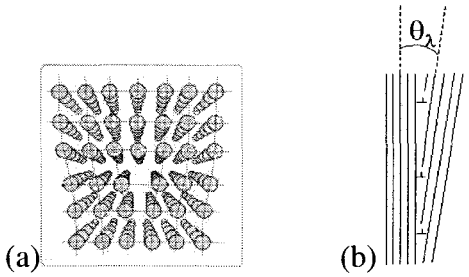

Figure 6. a) Atomic Configuration of an Edge Dislocation b) Edge Dislocation Arrangement for a Lower Energy Configuration.

More specifically, the residual compressive stress regions will reduce the residual tensile stresses of the adjacent dislocation. The shear stresses of opposing directions will negate each other as well. When dislocations align themselves in this manner, the crystals on either side of this boundary slope are misoriented with respect to each other. These well-defined boundaries are called subgrains. Typically, this misorientation, or θ_λ, is on the order of 1° in the five-power law regime. [2] Dislocations can also assume a more poorly arranged array of dislocations, called cell walls. Misorientation angles of cells are usually less than just one-tenth of a degree and are difficult to measure.

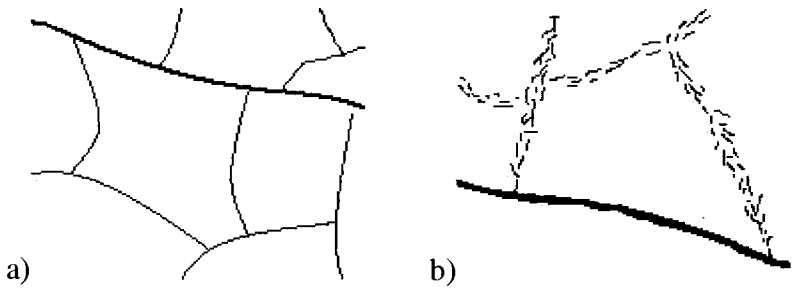

Figure 7. a) Subgrain boundaries b) Cell boundaries

There is some controversy as to whether copper forms subgrains or cells. TEM analysis of aluminum (high stacking fault energy), as shown in Figure 8, and austenitic steels (low stacking fault energy) samples shows a well-defined subgrain boundaries. Some of the most frequently referenced Cu work suggests that well-defined subgrains do not form in Cu, like in metals in the five-power law regime. Cellular tangles of dislocations form instead. Others [17,22] appear to suggest that well defined subgrains form, although the micrographs can be ambiguous. Terms such as "cells," and "subcells," and "subgrains" are all used. Again there is a conflicting work in the

literature as to the nature of low-energy dislocation configurations in Cu in five power-law creep.

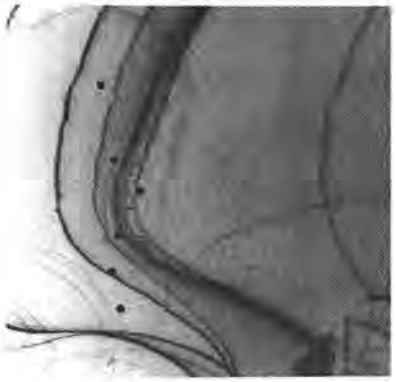

Figure 8. Subgrain Boundaries in Aluminum at 371°C $\dot{\varepsilon}$ =5.04x10^{-4}s^{-1}.

Regardless of which structure copper develops, as the crystal is further strained several of these subgrain boundaries develop and a three dimensional array developes within the grain. An illustration of this is shown in Figure 9. As the crystal is further strained these subgrain boundaries, as well as the grain boundaries, begin to increase in dislocation density, ρ_{ss}. Dislocations are created within the interior regions of subgrains and migrate towards the boundaries, becoming pinned and leaving the interior of the subgrains with a relatively low dislocation density.

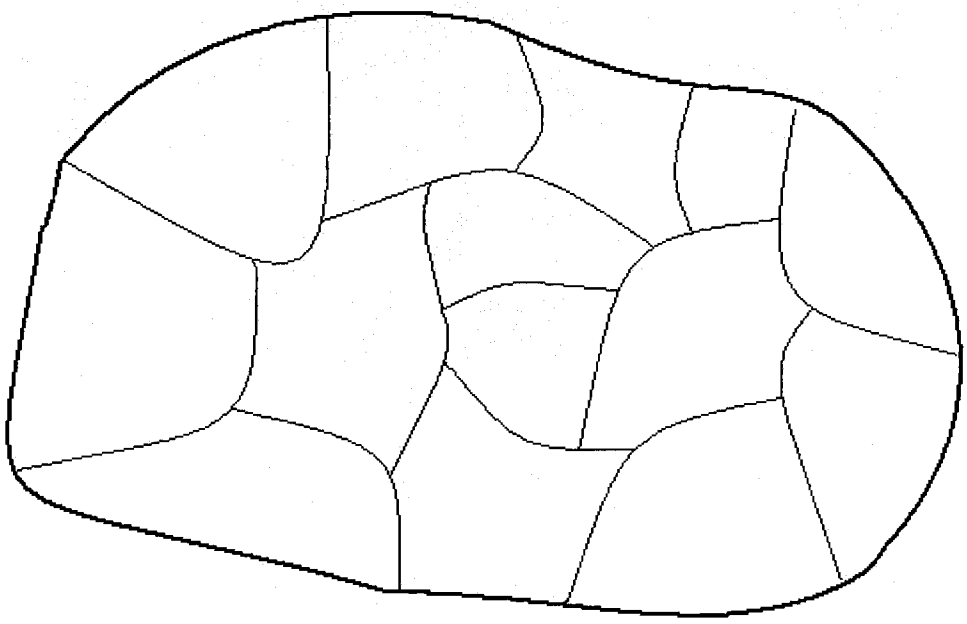

Figure 9. Subgrain Diagram Size Behavior

Because of the difficult nature of testing copper there is a relatively small amount of data in the literature for measurements of subgrain sizes and dislocation densities. Experiments of other metals show a subgrain size trend of:

$$\frac{\sigma}{G} = C_2 \lambda^{-1} \tag{11}$$

This equation gives a general relationship between subgrain size and applied stress. It is not an equation defining the relationship between temperature and strain rate with subgrain size. Figure 10 shows a plot of previous works reporting steady state subgrain values for copper.

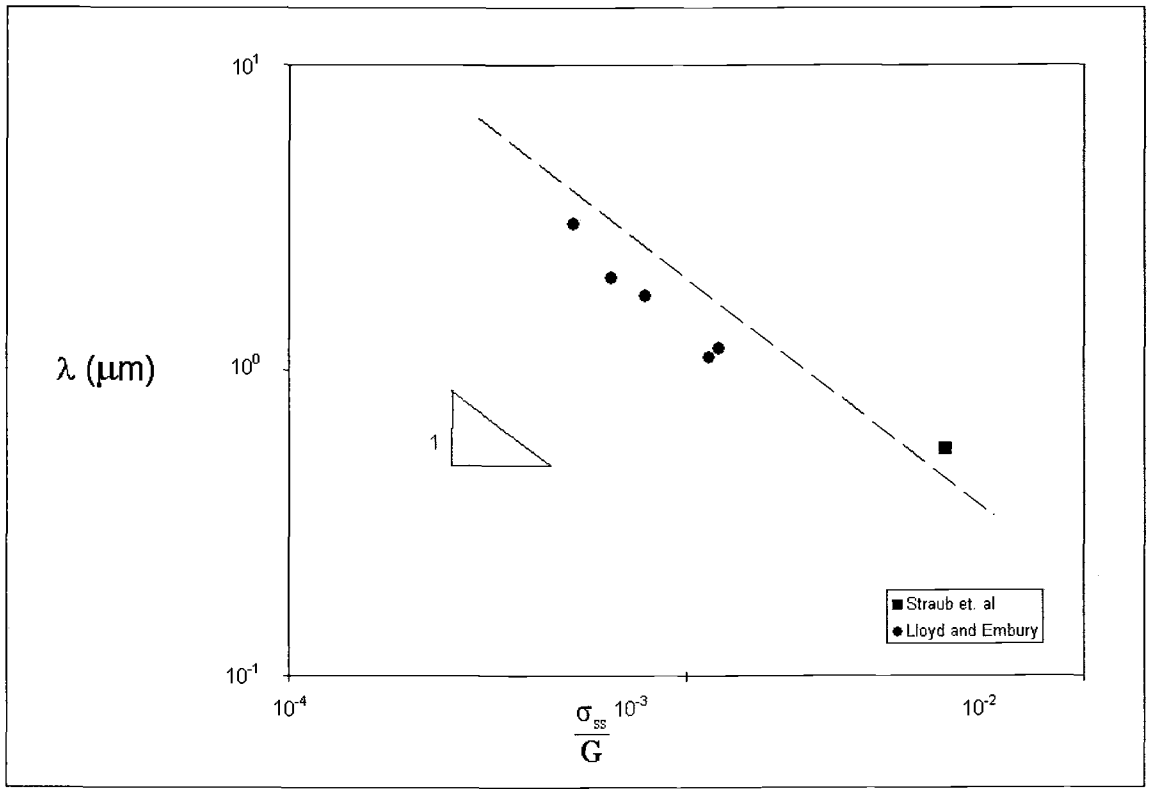

Figure 10. Steady State Subgrain Size vs. Modulus Compensated Steady State Creep Stress In Pure Cu

2.6 DISLOCATION DENSITY

As the material is plastically deformed during primary creep, the total dislocation density increases both within the subgrain interior and boundaries. Some dislocations are incorporated into subgrain/cell walls, while others develop into a Frank network of dislocations within the subgrain interior. It is not known which of these features are responsible for strength. The nature of any strength provided by the cell walls is also controversial. Some believe that a back stress, or long range internal stress, is caused by bowed subgrain boundaries and some believe in a long range internal stress from a composite model. The composite model involves hardened subgrain boundaries (high

dislocation density) and softer (lower dislocation density) regions that will yield at differing stresses. Leading to a heterogeneous stress state.

Knowing that dislocations are the influential factor to the strength of a metal it is helpful to understand the mechanisms of dislocation multiplication as well as the multiplication rate. The analogous equation to (11) for the dislocation density is:

$$\frac{\sigma_{ss}}{G} = C_3 \rho_{ss}^{\frac{1}{2}} \tag{12}$$

This is often confused with:

$$\sigma = \sigma_o + \alpha G b \sqrt{\rho} \tag{13}$$

which refers to strength at a fixed T and $\dot{\varepsilon}$. This is unlike Eq. 12 which shows the steady state dislocation density. Data from this study will be the only data available.

2.7 RELATIONSHIPS OF VARIABLES

The five-power-law creep is a complex system involving an interesting mix of variables. There are four classifications of variables that are involved in this system; they are deterministic, consequential, dependent, and constants. A diagram illustrating the relationship of the variable is shown in Figure 11.

The deterministic variables are the defining elements of a creep system. These are the conditions that can be affected during testing. They are stress, strain-rate, and temperature. A creep system is defined by having a combination of temperature and either constant stress or constant strain-rate, in which both can be variable. If stress or strain-rate is chosen the other will become a resultant effect of the system. This resultant effect is due to the nature of strained metals.

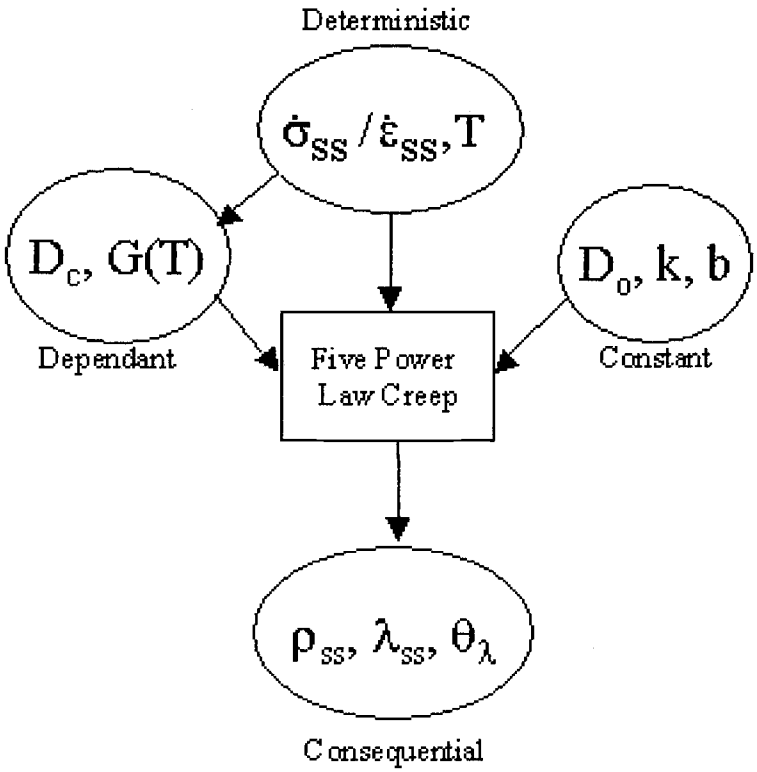

Figure 11. Relationships between variables.

Influential factors, or dependent variables, include shear modulus and activation energy for diffusion. It must be noted that they are not listed as deterministic because they do not themselves affect the resultant or consequential effects, but rather they play a role in further defining the nature of the creep system. They also are important in the normalization of data in plots. In addition to not having a defining role in the nature of the creep system the dependent variables are themselves partially dependent on the deterministic variables. As discussed earlier, modulus is a function of temperature and the activation energy is a dependent on both temperature and stress.

For most applications the shear modulus is usually considered to be a material property and constant, but as calculations have shown its value can drop by as much as 25% over the range of temperatures within five-power-law creep regime. Also, most assume the activation energy for diffusion is constant and equal to lattice self-diffusion

energy, but it has been shown that there is an increase in activation energy as temperature increases[7] in the five power-law creep regime. In addition to temperature effects, Raj and Langdon have shown stress-dependence. It is because of these two effects that activation energy is described as a dependent variable. However, for simplicity this paper will consider the activation energy to be constant and equal to that of lattice self-diffusion activation energy as is usually observed in five power law for other materials..

The last category of variables that influences creep is one that are considered constant with respect to the testing conditions. This category includes the diffusion coefficient, Boltzman's constant, and the Burgers vector, etc.

For a given system of defined deterministic variables, which influence dependent variables, and the normal constants, a series of resultant effects in the crystal will occur. These effects are to be called consequential variables, because they are a consequence of testing in conditions and not independent of the system. As the material strains during high temperature testing a sub-structure or microstructure will develop within the grain. The material properties develop due to the test conditions include dislocation density, subgrain size, subgrain misorientation, and (some believe) a long range internal stress.

2.8 INTERNAL STRESSES

In the past, many have tried to define the mechanics of creep deformation in crystal structures. As mentioned earlier, there are two theories proposed to describe the microstructural strain effects. While both describe residual strain effects in the crystal they differ in theory.

One of the most predominate theories involves what is called internal, or "back stresses." Mughrabi [22,23] describes the case where "hard" (high dislocation density walls or cells) and "soft" (low dislocation density) elastic-perfectly plastic regions are compatibly sheared in parallel. Since the hard regions will yield at a higher stress than the softer regions, a heterogeneous stress-state (subgrain walls at high temperatures) within the cell walls develops. As the hard and soft regions are unloaded in parallel the hard region eventually, while its stress is still positive, places the soft region in

compression. The total or average stress may still be zero across the cell or subgrain, but the residual stresses in the hard regions are predicted to be positive and negative in the soft regions.

The second concept of internal stresses involves the dislocation configuration. This model was proposed by Nix and Ilschner[12], Argon and Takeuchi [24], and Gibeling and Nix[25]. With this model, the subgrain boundaries that form from dislocation reaction, bow under action of shear stresses and this creates relatively high "long range" internal stresses. The high stresses in the vicinity of the boundary are suggested to be roughly a factor of three larger than the applied stress. On unloading, a negative stress in the subgrain interior causes reverse plasticity (or anelasticity). There is a modest anelastic back-strain that is associated with this backstress.

Originally, the concept of internal stresses was developed to help explain the Baushinger effect. The Bauschinger effect, shown in Figure 12, describes the condition in which a metal hardens after some plastic strain, and on reversal of the loading direction, the metal plastically flows at a stress less in magnitude than in reached in the forward direction. This is contradictory to what would be expected based on isotropic hardening. This effect is well characterized, but the exact mechanism is not yet fully understood. Long-range internal stresses would allow for an explanation, because the soft region would already be in a residual compressive stress, thereby lessening the required load to reach the yield stress.

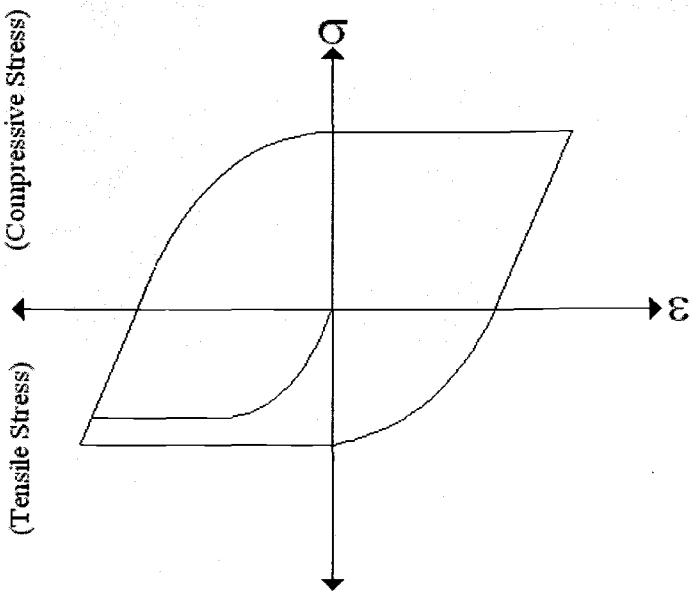

Figure 12. Bauschinger Effect in Al Single Crystal at 771°C.

However, many feel internal stresses are not the cause for the Bauschinger effect, if they even exist. Sleeswyk et. al. [26] have concluded that internal stresses are not the determining factor, but an Orowan type mechanism is occurring. Their suggestion is that upon loading, gliding dislocations encounter increasingly effective obstacles and the stress necessary to activate further dislocation motion, or plasticity, continually increases. On reversal of direction of straining, however, the dislocations will need to only move past those obstacles they have already surmounted. Thus, the flow stress is initially relatively low.

This discontinuity in theory over the mechanics of Bauschinger effect is an example of a significant controversy in strength of materials. The continuing argument of whether internal stresses do exist extends quite deeply in to strength of materials. Developing a theory that not only describes the Bauschinger effect, but also the details of monotonic deformation is important for the metalurgical community.

In summary, it is unclear whether the hetergenities (cells, subgrains) are responsible for the five power-law-creep strength or whether the networks of dislocations are responsible. In as much as subgrains or cells are responsible, the nature of the influence is unclear; the role of long range internal stresses, if it exists, in five-power-law creep is unclear.

2.9 ELECTRON MICROSCOPY AND X-RAY DIFFRACTION

To help determine the nature, or existence, of internal stresses, several types of microscopic analysis have been performed on materials with heterogeneous microstructures. Creep, because of its continued deformation and high temperatures, often develops well-defined dislocation structures and including subgrain boundaries.

In several influential papers, techniques were used to characterize the LRIS. One approach for validating the concept of internal stresses involves bulk-sample X-ray diffraction tests. Some of these test occur *in-situ*(or under loading), obtaining broadened diffraction peaks, representing the changing lattice parameters with increased dislocation density and, perhaps, dislocation configurations such as cells or subgrains, as illustrated in Figure 13. This broadened peak labeled "Observed Diffraction After Deformation," is believed by some [26] is the sum of two smaller (broadened) symmetric broadened peaks that represent the differing stress regions in the bulk sample.

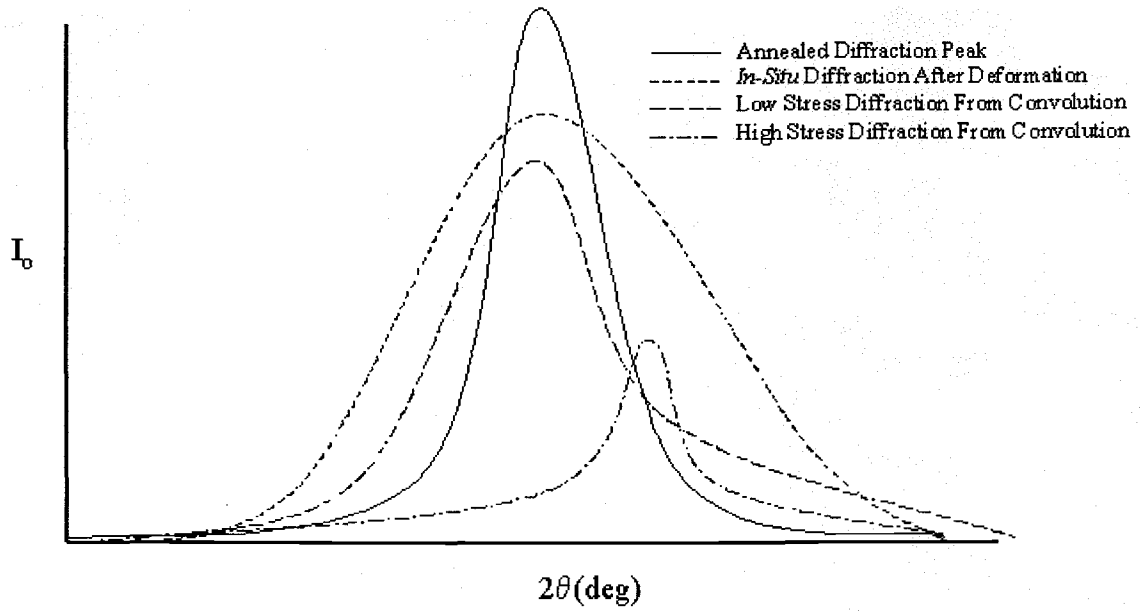

Figure 13. X-Ray diffraction peaks

As the material is deformed there is also asymmetry. Some have "analytically deconvoluted the asymmetric peak into two symmetric peaks. The peak labeled "low stress diffraction peak" represents the portion of material of low lattice parameter change, while the smaller peak, labeled "high stress diffraction peak," represents the regions of an increased lattice parameter change, as a consequence of higher local peak stresses. The higher stress region is associated with the dislocation heterogeneity such as a cell wall or subgrain boundry.Straub et. al [27] and Borbely et. al [28] performed these tests and were not able to show direct evidence of this effect. Unfortunately, X-ray diffraction analysis can only analyze bulk samples, and as such cannot determine the lattice parameter at individual boundary or individual cell interior.

In a similar experiment, Mughrabi [22] performed a neutron irradiation experiment of strained material and showed what has been interpreted as evidence of internal stresses. This work measured local stress by bowed dislocation, although the low

stress regions may have had unstable configurations of dislocations and may not have been reliable in assessing the stress state.

It has been found that unloaded bulk specimens will show broadened, asymmetric diffraction peaks. Thus, if the asymmetric peaks indicate residual stresses, then it might be possible to measure LRIS using electron microscopic techniques on unloaded specimens. One method that will characterize the residual stresses in a crystal is convergent beam electron diffraction (CBED). As shown in Figure 14, CBED beams differ from a wide parallel beam TEM analysis, in that they can be as narrowed to a beam as small as 20nm, allowing for a small sampling of the material. Diffraction patterns from these finely tuned point reflections will project on the diffraction plane as spheres, which are crossed by HOLZ (higher order Laue zone) lines, as seen in Figure 15. By precisely comparing the measured position of the HOLZ lines to calculated theoretical positions it is possible to quantify the change in lattice parameters, and thus internal stresses. With accurate methods it is possible to detect even small changes of $\pm 10^{-5}$ nm and crystal misorientations of 0.01°.

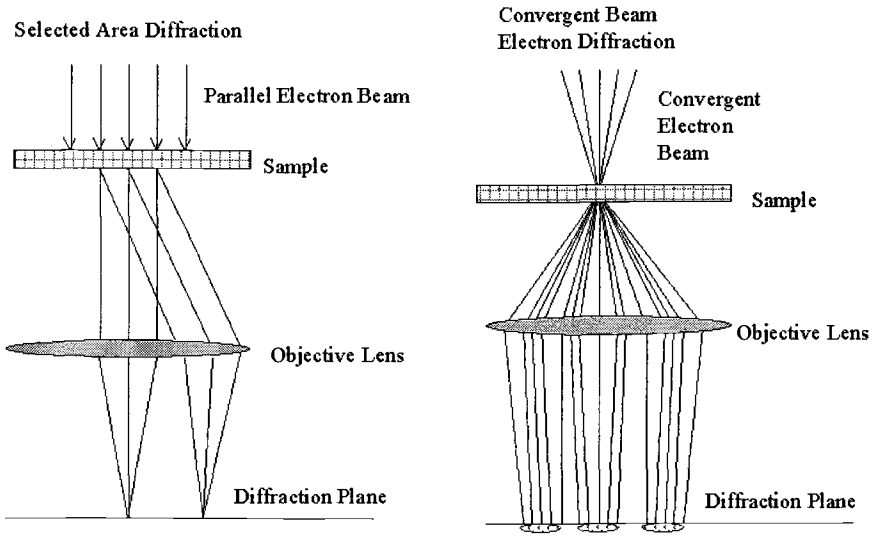

Figure 14. (a) TEM and (b) CBED beam.

By traversing the beam across a subgrain and measuring the lattice parameter for evidence of internal stresses it is possible to develop a stress profile. This process is shown in Figure 15, with each black dot representing an analysis point.

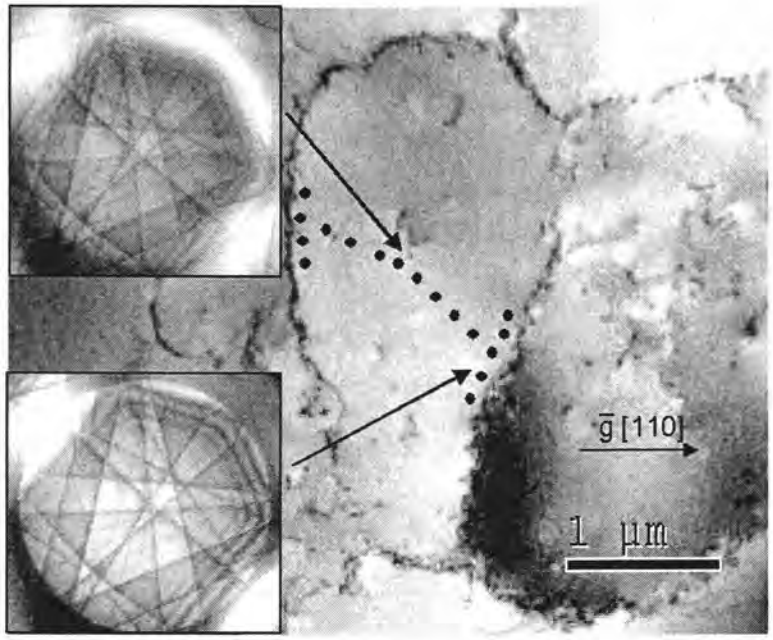

Figure 15. CBED pattern with HOLZ lines.

Despite the benefits of using a narrow beam there are negative issues surrounding CBED analysis. TEM or CBED analysis requires foil samples of small thickness. In electropolishing the sample to this thickness it might be possible for the internal stresses within the subgrain to relax, negating the strain measurement such as dislocation emission.

To measure if this relaxation occurs, dislocation densities found in the subgrain boundaries and interiors found in thin CBED sections can be compared to those found in thicker sections, where relaxation is unlikely to occur. If dislocation densities are similar, it is reasonable to assume dislocations are not ejected from the subgrain boundary and thus relaxation from the source has not occurred.

In more recent fatigue experiments on Al, Kassner et. al [29] show the stress to be uniform across the substructure and equal to the applied stress. This result contrasts with the reporting by Morris and Martin [30,31] of values of local stress ranging from equal to up to 20 times the applied stress in aluminum 5% Zn based on precipitation pinning of dislocation loops.

2.10 RECRYSTALLIZATION

The steady-state creep discussed so far is a balance between dynamic recovery (dislocation annihilation and subgrain boundary formation) and hardening. Another problem that occurs in creep testing of many metals is dynamic recrystallization (DRX), another restoration mechanism. This has been proven quite a sore spot for many researchers because five-power law creep is valid for dynamic recovery only. The restoration mechanism of recrystallization may preclude a study of five-power law creep because it may negate any of the usual steady-state subgrain or dislocation structure that develops during stage II creep. Secondary creep researchers, doing creep studies, must take care to avoid this. There are several indicative items for DRX has occurred.

The first involves an inspection of the conventional strain vs. time plot. Barrett [4] illustrates a plot on which DRX occurs. An unstable stage II, as seen in Figure 16, the suddenly increase of strain rate is indicative of DRX.

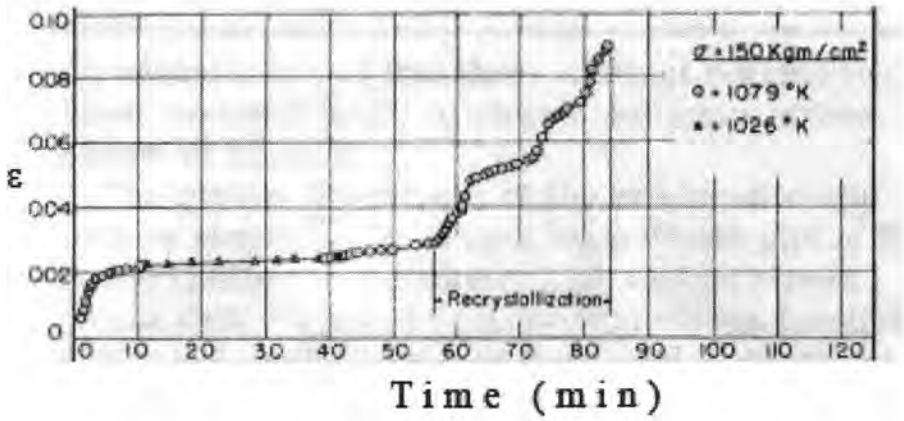

Figure 16. Creep plot with DRX occuring. [4]

A second procedure to determining if DRX is occurring within a sample is to make a comparison of the gauge section to the grip. Because the DRX is stress activated, and the thicker grip section has a lower stress, there will be no recrystallization in the grip. If DRX occurs in the gauge the grain size will be different than the grip. A comparison of grain sizes can help eliminate, or show DRX.

For copper there is some ambiguity as to the regions in which recrystallization occurs. Pahutova et. al [10] claimed that DRX is not observed below 1025°K(750°C). However, in an earlier paper Barrett [4] describes a regime in which DRX occurs. While never quite stating a definitive region of temperature and stress conditions that lead to it, Barrett does provide two plots that help define the DRX regime.

2.11 OXIDATION

In addition to the problems involved with the activation energy and DRX, oxidation can render creep testing difficult. It is this specific reason that copper has had such a limited impact on the scientific data to this point. Other metals such as aluminum

and stainless steels, or zirconium grow an oxide layer that prevents continued oxidation of the samples, but copper's oxide layer is not as stable and will continue to grow unless certain precautions are taken. These precautions can include coatings such as gold or silver, testing in inert atmospheres like argon or nitrogen, or the most effective precaution, testing in high vacuum conditions.

Another issue with copper is the diffusion of oxygen into the bulk, and formation of small copper oxide particles that can affect the creep properties. These may form more substantially along grain boundaries, but also within the interior of the grains.

3. EXPERIMENTAL PROCEDURE

The elevated-temperature copper testing was initially expected to be performed at a constant strain rate on an Instron Model 8521. However, several problems with the testing fixture and temperature-control related problems forced moving to constant stress tests on a Satec creep-testing machine. The problems with elevated temperature testing of copper samples include oxidation and dynamic recrystallization often leading to premature fracture of samples.

Nine copper samples were tested at two different stress levels in an argon environment at 550°C. From the Satec-tested samples subgrain size, subgrain misorientation, and dislocation density measurements were performed using a transmission electron microscope (TEM). Convergent Beam Electron Diffraction (CBED) was also performed to measure internal stresses and lattice parameters. The TEM was performed on a Philips EM400 at the University of California at San Diego.

3.1 FLAT INSTRON SAMPLES

The original testing was to be performed on an Instron 8521 with flat dog-bone specimens, as shown in Figure 17. The samples were held in fixtures, as shown in Figure 18, designed originally for high temperature titanium tests. [32] The samples are held in the molybdenum fixtures by two means. The first is a titanium pin inserted through both fixtures and through the hole in the end of the samples. The samples are also friction griped by the serrated edges of the grips with the assistance of molybdenum bolts.

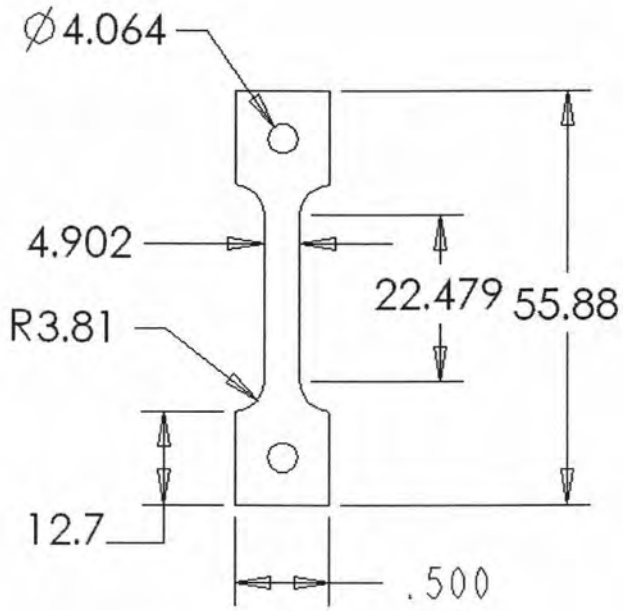

Figure 17. Dimensions of flat specimen. All dims in mm.

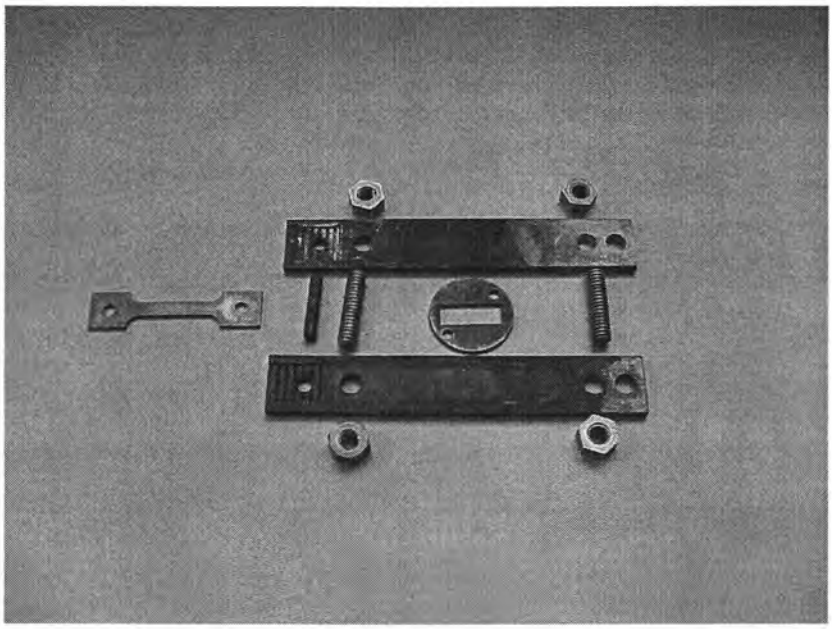

Figure 18. Molybenum Fixtures.

These fixtures and samples are assembled and installed on the Instron after chromel-alumel Type K thermocouples were tied using stainless steel wire. One particular problem was ensuring intimate contact of thermocouple beads with the sample. This is due to the relative bending ability of the thermocouple wire and bead size. After the specimen was mounted in the grips the assembly was moved to the Instron. Installing the testing assembly with the installed thermocouples without the specimen bending during was nearly impossible. Figure 19 shows an installed grips and specimen mounted in the testing fixture.

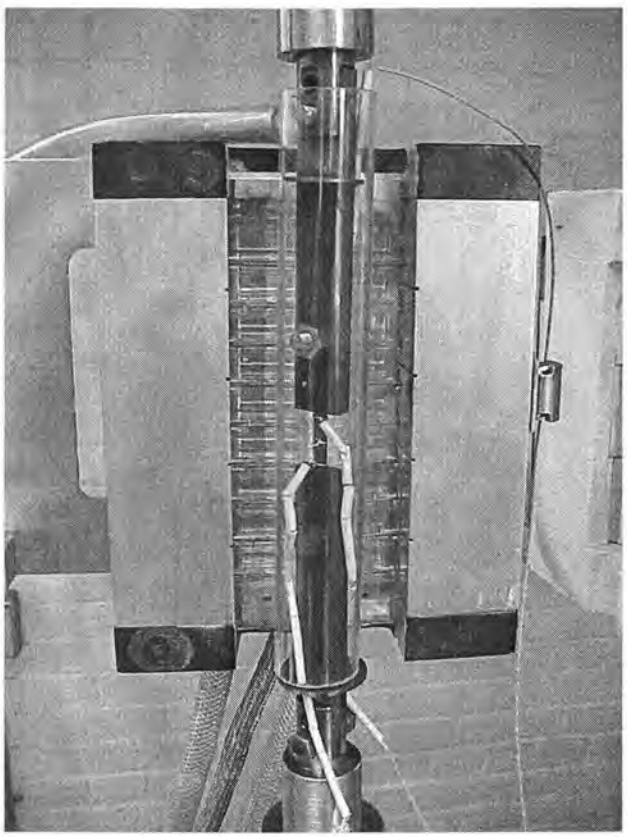

Figure 19. Installed Flat Specimen.

These samples were heated in a side-mounted RSI International halogen furnace. This furnace has three zones and heats the sample from both sides, ramping the current directly to the lamps controlled sample temperature.

Room-temperature argon is more dense then room temperature atmospheric gas, but at the given testing conditions the argon would be less dense then room temperature atmospheric gas. A quartz tube was constructed, in an effort to control oxidation, as shown in Figure 20. But it is unknown what happens to the argon gas as it passes through the chamber. Will it rise, causing upward chimney effects? Will it settle, drawing air into the chamber? Adding yet another level of complexity, the quartz chamber was designed with quenching holes to allow the sample to be quenched when testing was complete.

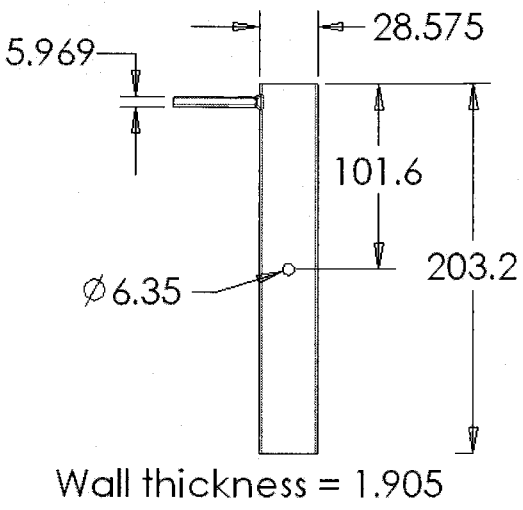

Figure 20. Quartz Chamber Dimensions. All dimensions in mm.

This testing procedure presented many problems. The most difficult involved the chamber ends and quenching holes open, making it difficult to maintain temperature and stable argon chamber conditions. Inside the chamber there were unstable argon flow rates, chimney effects due to thermal expansion of the argon gas, molybdenum oxidation buildup (MoO_3) from the testing fixtures, and continued copper oxidation. All of these problems would cause the rate of heat flux to the sample to change unpredictably, and therefore made it difficult to maintain constant temperature. The copper oxidation was particularly interesting because the initial copper sample was polished, having a low emmissivity, of ~0.1. As the sample oxidized the emmissivity increased ~0.8 causing changing rates of sample heating. This caused significant problems maintaining consistent testing temperatures.

One of the major objectives of these creep tests was to quench the samples in the stage II creep regime. The quartz chamber presented several difficulties in accomplishing this. The first difficulty came with the dimensions of the quenching holes. Trying to aim the jets of water through the small holes proved to be quite a challenge. Larger holes could be added, but this led to increased oxidation due to escaping argon. It was found that the water injected into the chamber could vaporize before it would reach the sample with the quartz chamber at an elevated temperature.

Stainless steel plugs were made to cap the bottom and top of the chamber, and the quench holes were allowed to vent freely to compensate for the argon problems. However, this did not completely eliminate chimney induced oxidation effects. To combat the problems involved with the quenching water, a series trial aiming devices were built and abandoned because of the inability to correctly align the jets with the quench holes. While some these problems are very common with copper, there were other issues that warranted a change in testing methods or conditions. One of the more significant problems involved possible dynamic recrystallization.

It has been observed that testing at temperatures over 600°C, recrystallization is pervasive and inhibits the development of a steady-state dislocation substructure that is a balance between hardening and dynamic recovery as the exclusive restoration mechanism. It was decided a lower testing temperature of 550°C should eliminate this

problem. A literature review and suggests that recrystallization should is not a problem below 600°C. [4,10]

Another problem involved the microstructure and geometry of the sample. Many of the samples had grain sizes widths greater than the sample thickness; creating scatter in the mechanical data. It was decided that larger round samples would help with the oxidation difficulties, limit grain sized effects and bending problems.

3.2 CYLINDRICAL INSTRON SAMPLES

This second series of tests using round samples were again performed on the Instron 8521. The samples, shown in Figure 21, were machined from 99.998% pure copper rod, with trace elements listed in Table 1. The samples were screwed in stainless steel fixtures. The samples with thermocouples were installed, as shown in Figure 22. With changes to the sample geometry, testing fixtures were changed as needed. To accommodate the change in fixture design an enlarged quartz chamber was constructed. End caps were not needed because of the good fit of the quartz tube relative to the testing fixtures.

Table 1. Trace Element Analysis

Cu	Pb	S	Bi	Cd	Se	Thalium
99.9985	<7ppm	<5ppm	<2ppm	<1ppm	<1ppm	<1ppm

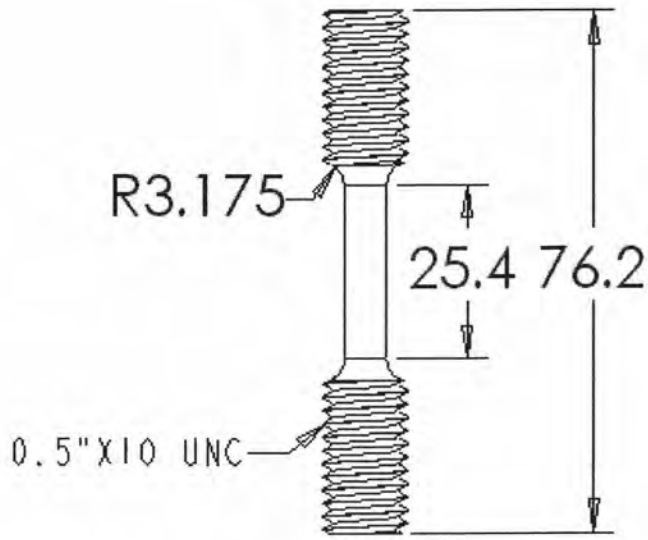

Figure 21. Cylindrical Sample Dimensions. All dims in mm.

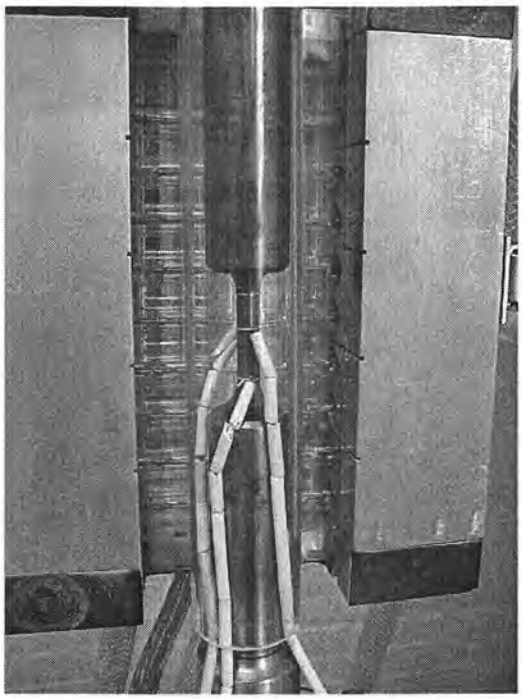

Figure 22. Installed Cylindrical Sample.

Changing to a larger sample is believed to help with the oxidation and grain size effects. Initial testing with the larger samples showed less penetration of oxidation through the sample and fewer cracking along grain boundaries after quenching. Additionally the rectangular samples showed signs of through sample cracking due to oxidation before creep tests were complete.

There still was an extensive problem with obtaining a proper quench when testing was completed. Chimney effects were still causing enough oxidation to create an uncertainty with the stress, as well as continuing emmissivity effects. After a discussion with B. Wilshire [33] it was recommended that, during annealing, oxygen effects and dynamic recrystallization be eliminated. Their recommendation was to anneal in an vacuum of at least 10^{-3} torr. Additional recommendations were to make efforts to create a stable argon environment during testing and maintaining a testing temperature below 600°C, both of which were goals we were working towards.

3.3 ANNEALING

It is commonly known that copper is especially susceptible to oxidation problems during annealing and during elevated temperature testing, as mentioned earlier. Formation of oxide particles can further cause early fracture and preclude sufficient strain to achieve a genuine steady state that is a balance between hardening process and dynamic recovery. Consequently, the samples were annealed in a vacuum furnace at the Dept. of Energy Albany Research Center, Albany, OR. Annealing conditions were 7.36 x 10^{-4} torr and 1000°C for 10 hours. Pre and post anneal grain size data is shown in Table 2.

Table 2. Pre and Post-anneal grain sizes.

Pre-Anneal (mm)	Post-Anneal (mm)
0.08	1.26

3.4 SATEC TESTING

A change was made from the Instron 8521 to the Satec Creep Tester because of the greater ease in controlling the testing atmosphere. Making this change required yet another change the samples dimensions to work with the extensometer installed on the Satec. The material used for this series of experiments was a high purity copper rod provided by The Metron Corporation. Chemical analysis shows the material to be 99.998% pure; with a trace element analysis shown in Table 1. Samples were machined to the dimensions shown in Figure 23 using small final cuts (<0.0005/cut) to avoid excessive cold working.

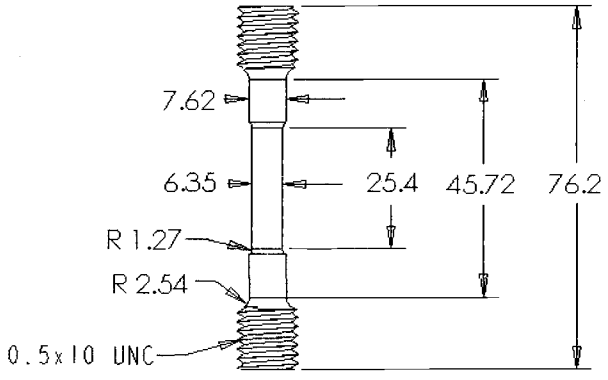

Figure 23. Satec Sample Dimensions. (all dims in inches)

All mechanical testing was performed to ASTM standards E633-95, E8-99 and E6-98. A detailed checklist of procedures is included in Appendix A. The mechanical tests were performed on a SATEC model UC creep testing machine. This particular creep-testing machine has a constant load lever action arm. There are two possible lever settings on the Satec model UC creep machines, 3x1 and 8.16x1. Because the samples were relatively soft and would be deformed under low stresses the 3x1 lever arm setting was chosen.

Sample extension was measured using a Precision Instruments LVC model L1-12 on the 0.5" setting. The strain was measured using a Measuretron Extensometer Series 4112.

Since the testing required constant true stress, a method of weight removal was devised to accomplish this during testing. Based on the assumption that the sample will remain a constant volume and does not neck during testing, Equation. 11 was derived relating the load needed on the load tray, F_{To}, to the voltage readout from the extensometer, v_t. .

$$F_T = \frac{\pi \sigma_{ss} d_o^{\,2} l_o}{12\left(\frac{v_t - v_{to}}{C_v} + l_o\right)} \tag{14}$$

where v_{to} is the initial voltage, l_o is the original sample length, d_o is the sample diameter, and C_1 on the 0.5" setting is 20 volts/inch. Since the samples were deforming at low stresses, calibrated 0.5lb weights of sand were taken off as necessary

For this series of experiments there were two particular stress conditions, 20 MPa and 40 MPa stress. Loads of 95 lbs and 48 lbs would be needed based on the lever arm and sample dimensions.

The heating of the samples was accomplished using a three zone Keith model KTVR3D 1850 furnace with a Eurotherm power supplies and controllers. Temperature measurements were made by three chromel-alumel Type K thermocouples in direct contact with the specimen. Operator control was occasionally needed to adjust the temperature controls as the conditions in the chamber changed periodically. Some of the

changes in chamber conditions were attributed to changing of argon bottles, oxidation changing the emissivity of the sample, and oxidation flakes blocking radiative and convective heat effects from furnace.

Recording of temperature data was accomplished using a Fluke Data Acquisition system coupled to a Macintosh SE utilizing Labview. Temperature control objectives of ±5°C were attempted during any experiment. Results showed ±5°C on all tests except Copper VI in which the temperature fluctuation were±10°C.

One particular problem with this model extensometer is slippage or sliding of the grips relative to the sample. Several trial tests were performed on low purity samples to ensure that there would be no relative motion between the grips and the sample. It was found that if the grips had been sufficiently tightened this problem can be avoided.

Several techniques were employed to avoid excessive oxidation of the Cu specimens. First, oxygen "getter" strips made from 0.003" titanium foil, and placed in the testing fixtures to attempt to deplete the chamber of oxygen during heat up. Second, caps for the top and bottom of the chamber were made from aluminum foil to limit chimney effects from the flow of argon. Lastly, argon gas was allowed to flow into the chamber at the maximum allowable rate of 30 cfm (cubic feet per minute).

The Keith furnace had no fittings for gas supply. A solution using the top thermocouple port as a gas port was employed. A stainless-steel argon supply tube was inserted through this hole. A thermocouple was tied to the load train and positioned in the upper oven region to allow measurement of the top furnace zone, in order to maintain temperature control in the upper oven zone.

The sample was quenched after testing. This was difficult to accomplish because the sample could not be removed from the load train. So, the furnace door was opened and water was squirted from a syringe on the sample, as the applied load was removed. This quenching occured within 5 seconds of removing the applied load. Dousing with water was continued due to the conduction of heat from the load train to the sample. The sample post quench temperature never went exceeded 120°C on all experiments.

3.5 MICROSTRUCTURAL ANALYSIS

Microstructural Analysis was performed with assistance of Dr. M.T. Perez-Prado of UCSD and Mark Wall of Lawrence Livermore National Laboratory at the National Center for Electron Microscopy at Lawrence Berkeley National Laboratory. Copper foils were electropolished in a Fischione twin jet using 10% nitric and 90% methanol at -25°C. Foils were examined under bright-field (BF) conditions using a Philips EM 400 at 120 kV located at the University of California at San Diego.

Microstructure characterization included average subboundary misorientation estimation, average dislocation density measurement and average grain size determination. The misorientation of a subboundary, defined as the minimum angle of rotation that is necessary to bring the two crystals separated by the subboundary into coincidence, was determined in the following way. First, one of the two crystals was tilted to a <111> zone axis and the corresponding CBED pattern was recorded. Subsequently another CBED diagram was taken in the neighboring crystal and the shift of a particular intersection of HOLZ lines was noted. Average subboundary misorientations were calculated from 15 different measurements.

The density of dislocations not associated with boundaries was determined using the surface intersection technique [2]. <220> two-beam conditions were used to image dislocations.

CBED was also utilized to measure the lattice parameter in regions close to the subboundaries and in the center of subgrains with the aim of measuring residual stresses. A <411> zone axis with second order HOLZ lines were used. The accuracy of lattice parameter measurements was about ± 0.0001 nm or ± 0.03%. The CBED examination was performed at -175°C. The CBED beam diameter was estimated to be 80 nm. A large C2 aperture, 250 μm in diameter, was utilized which allowed a large angular view of the diffraction spots. CBED patterns were simulated using the software DF Tools 5.1 [1]. Reported error is associated with lattice parameter measurements from quality of the CBED pattern.

This page intentionally left blank.

4. RESULTS

Ten successful creep tests were performed, yielding seven successful creep data points. From these, two samples were sent to UCSD for microstructural analysis. The appropriate microstructure was analyzed using CBED and TEM from those two samples. Two additional samples, one from each stress, were polished to access DRX effects using direct optical metallography.

4.1 COPPER CREEP TESTS

Ten creep tests were performed at 550°C and 20 and 40 MPa constant true stresses. Figure 24 is a composite plot of each of the successful tests. The individual creep curves for each test are available in Appendix B. Steady state was achieved within a few percent strain and the classical stages of creep for pure metals was observed. Each of these samples was quenched within five seconds after unloading, and temperature control was better than ±5°C during testing, except Copper VI, in which temperature control was ±10°C. It is noted that of the ten tests performed only seven of the tests were used in Figure 24 and were viable for electron microscopy analysis. Table 3 shows the results of testing.

The tests labeled Copper I, Copper III, Copper VI, and Copper X were tested at a constant stress of 40 MPa and 550°C. The creep curves for these tests can be seen in Appendix B. The uniformity of the results confirms the accuracy of these tests. The tests labeled Copper VII, Copper VIII, and Copper IX were tested at a constant stress of 20 MPa and 550°C. The uniformity of the results also confirms the accuracy of these tests.

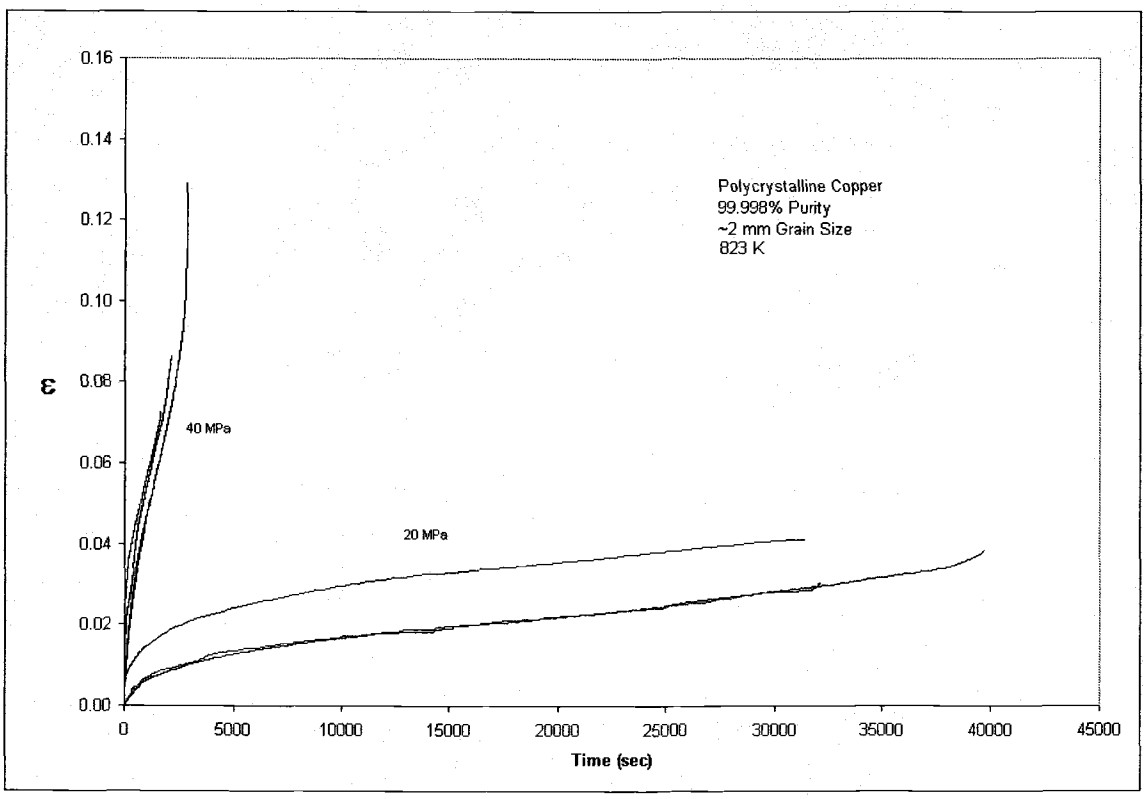

Figure 24. Composite Plot of Creep Curves.

Table 3. Results from Testing.

Test	Temp (K)	σ_{app} (MPa)	$\dot{\varepsilon}_{ss}$ (sec^{-1})
I	823	40	2.47E-05
II	823	40	8.45E-06
III	823	40	2.33E-05
IV	823	40	4.09E-05
V	823	40	8.45E-06
VI	823	40	2.48E-05
VII	823	20	5.70E-07
VIII	823	20	5.60E-07
IX	823	20	5.12E-07
X	823	40	2.50E-05

There are two explanations for the inclusion of only seven of the tests. The first is poor testing methods. On the test labeled Copper IV, close attention was not paid to the checklist of items needed for the tests. In a rush to start testing the argon was not turned on. Without argon flow the temperature profile is difficult to maintain, but more importantly the sample quickly oxidized at the elevated temperatures. This was not discovered until the quench of the sample was complete. This was a sobering lesson about following appropriate testing procedures and using a checklist. The test labeled Copper V has no results due to a problem with the data acquisition computer. The Macintosh SE computer used has a limited amount of RAM available for testing. On this particular test the wait step in the Labview program was set to zero seconds, so that a good resolution could be obtained during the test. However, when the test was complete and an attempt was made to save the data, the computer noted an error and quit the recording program. This unfortunate set back was another sobering lesson about knowing the limits of your equipment. On subsequent tests the wait step function in the data acquisition computer was set to zero during the beginning and end of tests to produce good resolution. While during the majority of the testing, a wait step ranging from one to five minutes was used, so that the number of data points would not overwhelm the computer.

For the test labeled Copper II, the strain rate does not fit with the other strain rates for that stress level. It can be seen in the plot appearing in Appendix B the tests appears to not have anomalous effects such as instrumentation or DRX. Upon inspection of the data from other similar stresses it is obvious that this data is somehow anomalous and can be discarded. Though the practice of excluding data is not normally acceptable, but with the good conformity of the three other tests of similar stress rendered this action.

Special attention must be paid to the creep plot for Copper VI because the changing strain rates shown are commonly associated with DRX. If this did occur, the CBED results are speculative. During this test, the temperature drifted likely due to an instrumentation error with the thermocouples. The drifting temperatures lead to changing

strain rates. Appropriate testing temperature was recovered quickly and the strain rate measured was for the time after temperature control had been recovered.

Figure 4 shows a normalized plot from previous works. Figure 26 includes the results of the present study. Most data sets have scatter. In the earlier work; on the order of 15% of the normalized strain value. The scatter for this data set is ±3.18% average strain rates for the high stress tests and ±5.66% for the low stress tests. This accuracy of results allows the data point to appear to fall on top of each other, as seen in Figure 25. There is good conformity with the slope trends between this study and other works. The slope for the other works is calculated as 5.61, while the general slope for this study is calculated as 5.50.

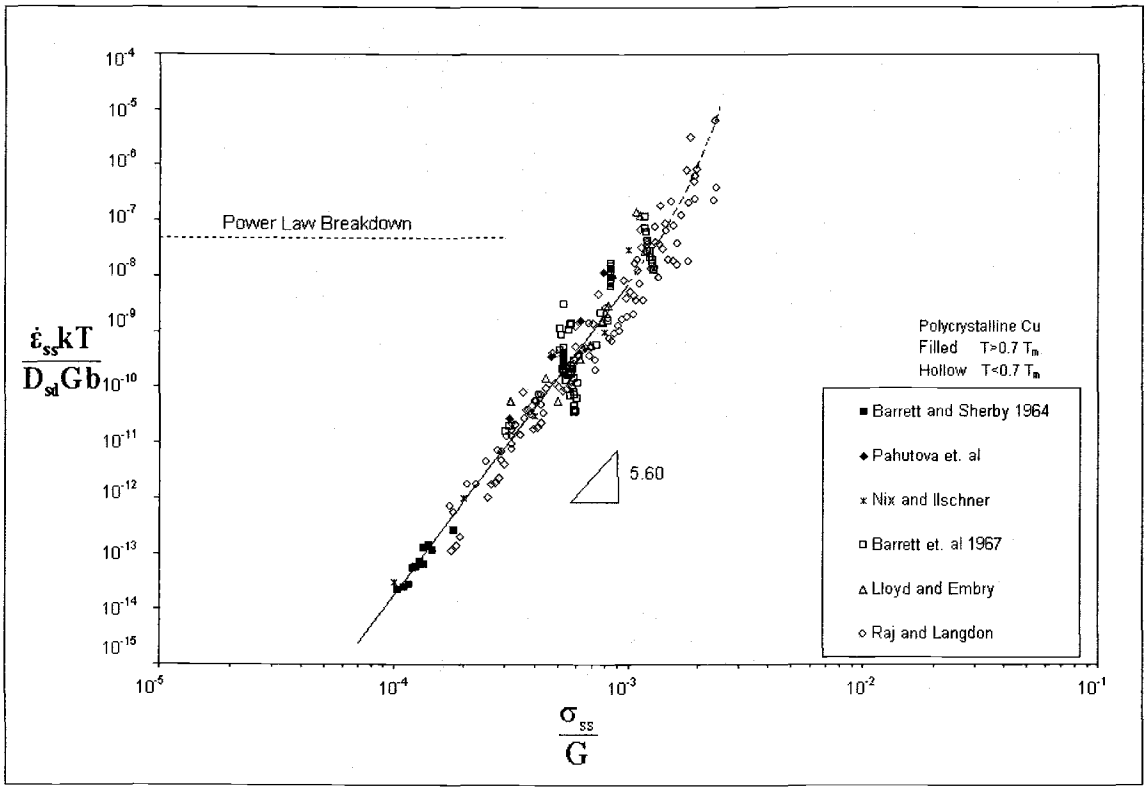

Figure 25. Normalized Plot With Data of This Study.

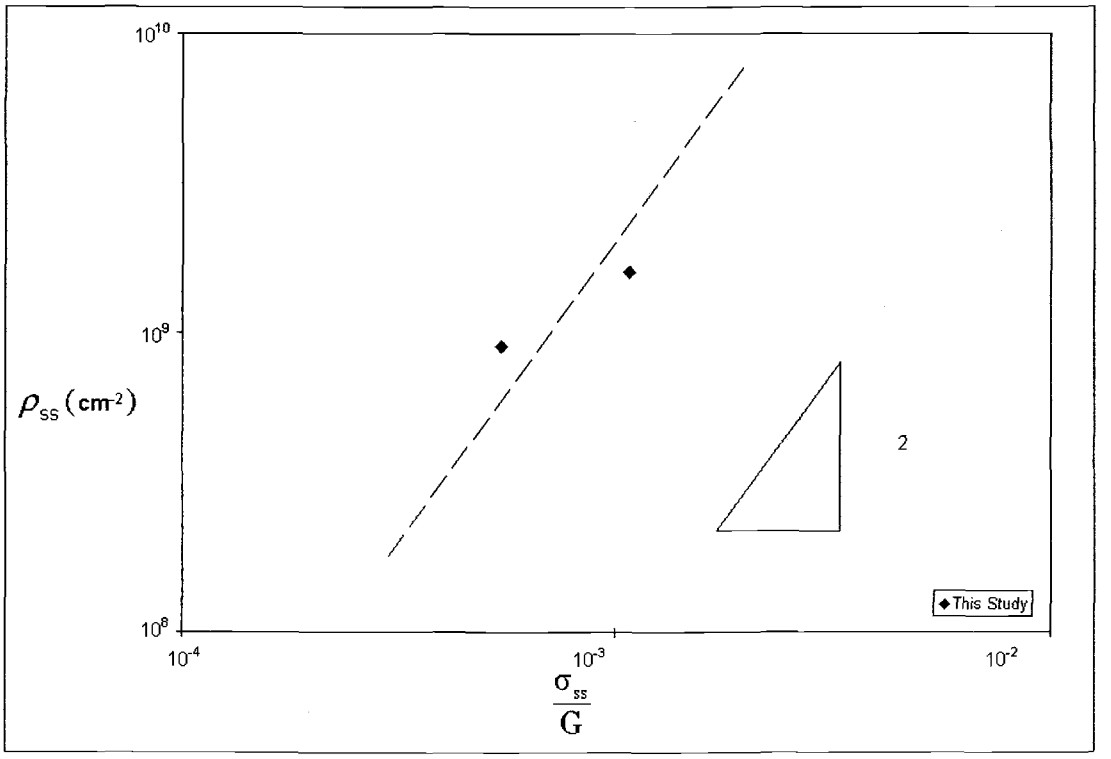

Figure 26. Dislocation Density.

It can be noted that the data from this study is below the general trend for data, but within the scatter band. Some possible sources for this include oxidation hardening, miscalculation of stress, consequences of testing at true stresses, data acquisition errors, or grain size effects. However, the testing methods are consistent with the ASTM standards and the equations for the calculations have been checked for errors and none were found. Leaving possible sources of error to include sample hardening from oxidation effects or using true stress.

4.2 MICROSTRUCTURAL ANALYSIS

Table 4. Results from Microstructural Analysis.

Test	Stress (Mpa)	Average Misorientation (deg)	Average Dislocation Density (subgrain interior) (cm^{-2})	Average Subgrain Intercept (μm)
Copper VI	40	0.18°	1.6×10^9	2.20
Copper IX	20	0.06°	0.9×10^9	2.86

The microstructure for the creep tested copper samples was analyzed at UCSD using CBED and TEM. Table 4 shows the results from this study. Six subgrain boundaries of two Cu TEM foils were traversed using CBED. The foils were extracted from specimens labeled Copper VI and Copper IX, deformed at 40 MPa and 20 MPa respectively.

The data in Table 4 clearly shows that Cu, like other pure metals, forms subgrains walls and a Frank network of dislocations within the subgrain interior. This is evidenced by the misorientation usually not evident in a "cellular" structure. Other evidence of this is illustrated in Figure 27. The subgrain boundaries do not appear to be as well defined as in aluminum in Figure 8. Rather, as described by Wilshire et. al [33], these heterogeneities are "less-well defined subgrain" walls. In addition, Figure 28 demonstrates that the data of this study are reasonably consistent with the expected trends of Eq. 9, for subgrain size versus the modulus-compensated stress, in view of the limited data. Though it should be noted that the subgrains of copper are not as well defined as other metals, aluminum in particular.

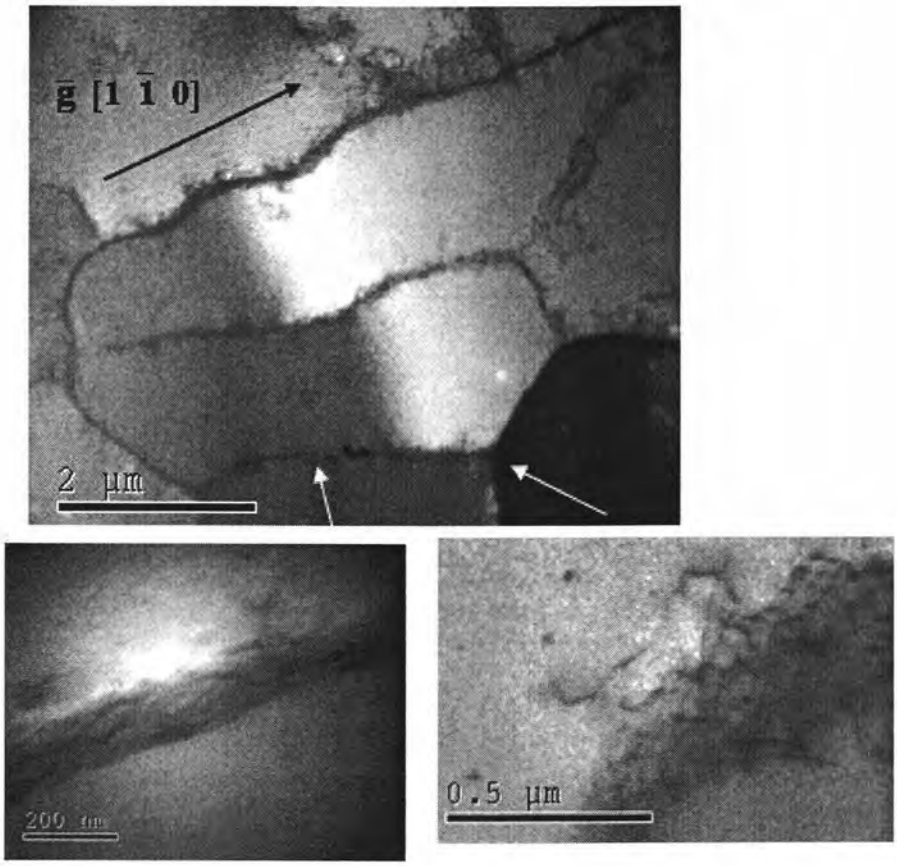

Figure 27. TEM of Subgrain Boundry in a Cu Deformed to 0.41 strain at 20 MPa and 823°K.

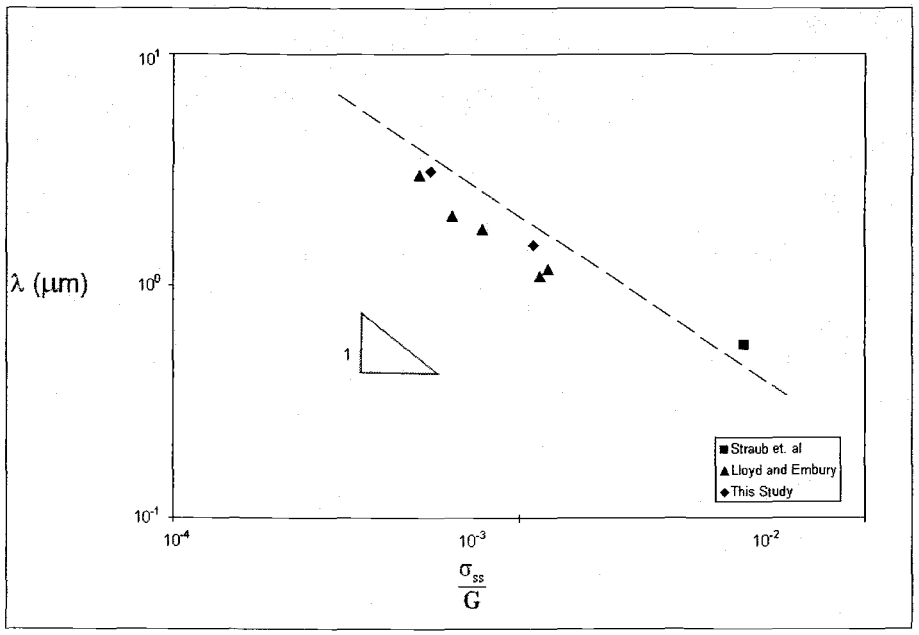

Figure 28. Modulus Compenstated Subgrain Plot, Size vs. Steady State Stress.

Figure 26 plots the data regarding the dislocation densities, and is reasonably consistent with the expected trends of Eq. 10, for the network dislocation density versus the modulus compensated steady-state stress, again in view of the limited data. It must be noted that the data for the high stress test, Copper VI, is speculative because data from which the high stress data was taken might have experienced DRX. DRX would have the effect of reducing dislocation densities.

The possibility is DRX in Copper VI is based on the conventional strain vs. time in Appendix B, as well as SEM image shown in Figure 29, that shows regions with fine grain size and other regions without subgrains. Notice the disparity in grain sizes between the sample in the upper ad lower sections in Figure 29. To rule out the possibility or DRX occurring in other tests, a grain size comparison of the grip and gauge sections were performed for Copper VIII and Copper X. Results of this are shown in Table 5. It can be seen that the grain sizes of the grip and gage sections are similar precluding the possibility of DRX. In addition to a comparison of grain sizes, an inspection of the other creep plots show no evidence of the "undulations" that are indicative of DRX.

Figure 29. SEM micrograph showing possible DRX.

Table 5. DRX grain size calculations.

	Copper VIII	Copper IX
Gage	0.87	1.01
Grip	1.01	1.24
Average	0.91	1.13

Figure 30 and Figure 31 show the lattice parameter and the stress calculations for 40 MPa and 20 MPa respectively. It was determined that the lattice parameter was unchanged within the interior of the subgrain and along the boundaries, within one beam diameter, or 80 nm, of the subgrain boundary. The measurements were also identical to

those of the annealed, stress-free, Cu polycrystals. Thus, within the accuracy of the lattice parameter measurements of the convergent beam electron diffraction, the creep-deformed substructure is stress-free. The (residual) stress error associated with the strain measurements is approximately ±30 MPa, or on the order of the applied stress.

As was described earlier, that using CBED might be speculative because foils might relax during polishing. As mentioned, a technique for determining if relaxation has occurred involves a comparison of the dislocation densities between thicker regions to the CBED regions. The dislocation density in the CBED measurements in the Cu specimens were 2.0×10^9 cm^{-2} and 0.8×10^9 cm^{-2} in the 40 MPa and 20 MPa creep tests. In comparison to the data shown in Table 4, it appears that recovery of the dislocation substructure does not occur in those regions where CBED was performed as compared to these relatively thick regions(0.2 μm) where the dislocation density measurements are performed. Of course, it must be considered possible that some, relatively small, residual stresses are present, but too small to be detected by CBED, or that residual stresses were once present but relaxed to an undetectable level.

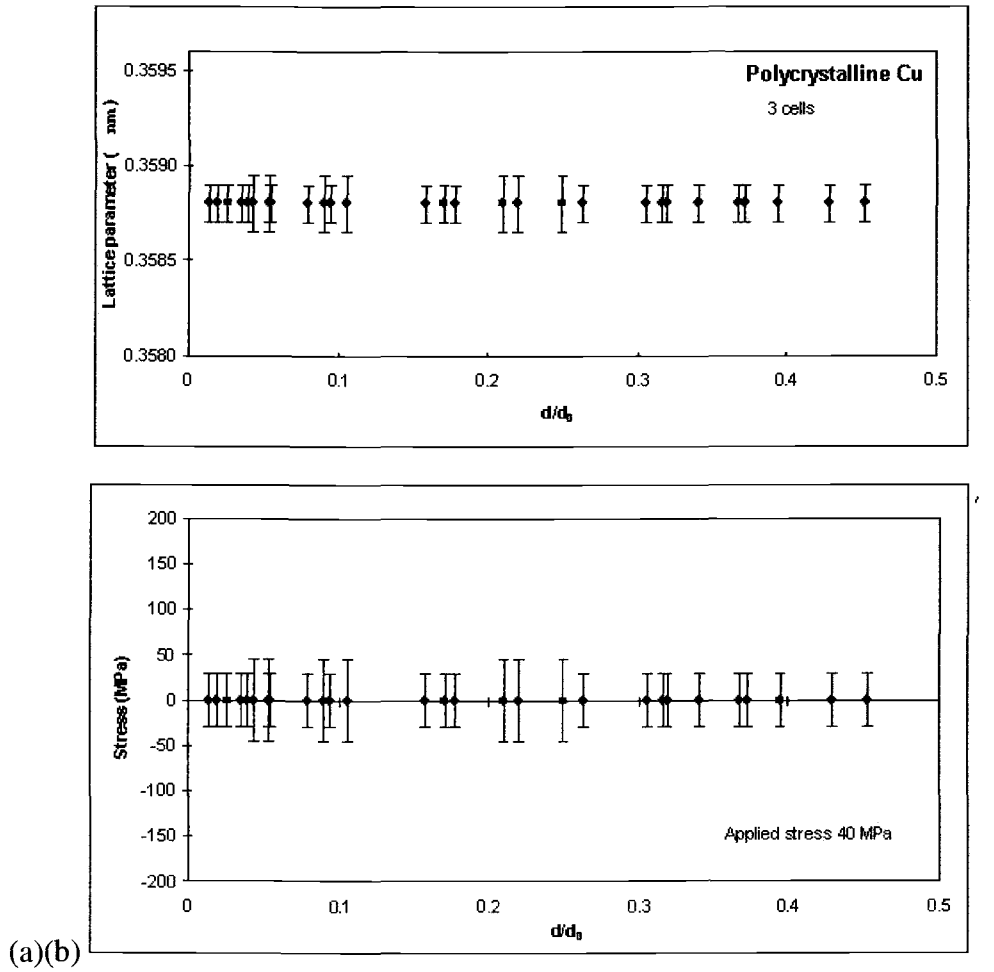

Figure 30. Lattice Parameter (a) and Corresponding Stresses (b) for High Stress Test.

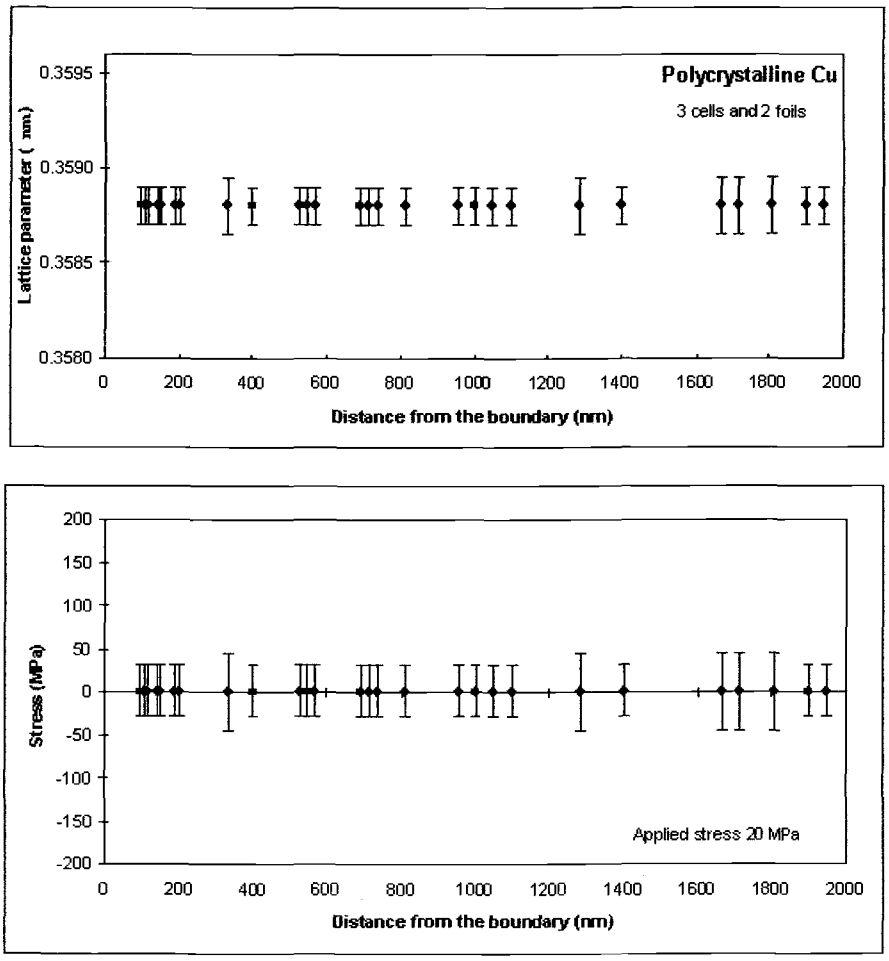

(a)(b)

Figure 31. Lattice Parameter (a) and Corresponding Stresses (b) for Low Stress Test.

5. CONCLUSIONS

1. Several copper creep tests were performed, at 20 MPa and 40 MPa at 550°C. Less well-defined subgrains form with less ordered arrangements of dislocations that in other materials such as Al, but more order, as evidenced by the misorientation angles, than cell walls. The trends of dislocation density within the subgrains and the average subgrain size is consistent with the other studies in terms of the value observed and the trends with the modulus compensated stress.
2. A clear trend of zero nominal stress in shown in CBED scans across subgrains. This leads to a conclusion that long range internal stresses, at least with the magnitude of the applied stress, are not present very near the subgrain walls or subgrain interior.
3. Discontinuous dynamic recrystallization (DRX) might have occurred in one high stress sample from which CBED specimens were obtained casting doubt on the resultant microscopy of that sample. DRX did not occur in other specimens where "normal" temperature control was observed.

REFERENCES

1. Staker MR, Holt DL. Acta Metall 1972; 20:(569-578).
2. Kassner ME; Perez-Prado MT. Prog Mater Sci 2000; 45:1-102.
3. Shewmon PG. Diffusion in Solids. Jenks, OK, U.S.A: J.Williams Book Company, 1983.
4. Barrett CR , Shearby OD. Trans AIME 1964; 233:1322.
5. Barrett CR , Shearby OD Trans. AIME 1965; 233:1116.
6. Parker JD, Wilshire B. Metal Science 1978; 453.
7. Raj SV , Langdon TG. Acta Metall 1991; 39(8): 1817.
8. Gilbert ER , Munson DE. Trans. AIME 1965; 233: 429.
9. Feltham P , Meakin JD. Acta Metall 1959; 7: 614.
10. Pahutova J, Cadek J , Rys P. Philosophical Magazine 1971; 23:509.
11. Retima M , Cornet M. Acta Metall 1986; 34: 753.
12. Nix WD, Ilschner B. In: Haasen; P, Gerold, V, Kostorz, G, editors. Strength of metals and alloys. Oxford: Pergamon Press, 1980.
13. Koster VW. Zeitschrift Fur Metallkunde 1948; 39(1): 1.
14. Lide DR. Chemical Rubber Company Handbook of Chemistry and Physics 79th edition. Boca Raton, Florida, USA: CRC Press, 1998.
15. Muchleisen EC, Barrett CR , Nix WD. Scripta Met 1970; 4(2):995.
16. Barrett CR, Lytton JL, , Shearby OD. Trans. AIME 1967; 23: 170.
17. Lloyd DJ , Embury JD. Metal Sci.1970; 4:6.
18. Coble CJ. Appl Phys 1963; 34:1679.
19. Brukner W. Phys Stat Sol (a) 1999;176:919.
20. Murty KL, Mohamed FA; Dorn JE. Acta Metall 1972; 20:1009.
21. Sherby OD, Burke PM. Prog Mat Sci 1967; 13:325.
22. Mughrabi H. Acta Metall 1983; 31:1367.
23. Mughrabi H. Materials Science Engineering A 1981; 85:15.
24. Argon AS, Takeuchi S. Acta Metall 1981; 26:1877.
25. Gibeling JC, Nix WD Acta Metall 1980; 45:1743.

26. Sleeswyk AW, James MR, Plantinga DH, Maathuis W.S.T.. Acta Metall 1978; 126: 1265.

27. Straub S, Blum W, Maier HJ, Ungar TT, Borberly A, Renner H. Acta Mater 1996; 44:4337.

28. Borbley A, Hoffman G, Aernoudt E, Ungar T. Acta Mater 1997; 45:89.

29. Kassner, ME, McMahon ME. Metall. Trans 1987; 18A: 835.

30. Morris MA, Martin JL. Acta Metall., 32 (1984) 1609.

31. Morris MA, Martin JL. Acta Metall., 32 (1984) 549.

32. Paddon, S. MS Thesis, Department of Mechanical Engineering, Oregon State University, Corvallis, OR, 1996.

33. Wilshire B. Private communication with M.E. Kassner, Nashville, TN, June, 2000.

34. Widersich HJ. J Metals 1964; 16:423.

APPENDICES

APPENDIX A

CHECKLIST FOR COPPER CREEP TESTS

SAMPLE PRE-TEST MATERIALS

1. Acquire sample rod material.
2. Machine samples to dimensions w/small cuts 0.0005" for the last 0.010" of machining to avoid excessive cold working.
3. Anneal samples 1000°C, 10^{-4} atm, and 10.0 hrs at Albany Research Center, Albany, OR

PRE-TEST CREEP MACHINE

1. Set lever arm to 3x1 setting.
2. Calibrate lever arm.
3. Check range of motion of weight tray elevator.
4. Check controlling switches for elevator control.
5. Change Inconel rods on load train to proper length a placing sample in center zone.
6. Calibrate oven Zone 2 and Zone 3 thermocouples.
7. Check oven controllers.
8. Check pressures on Argon bottles.
9. Install argon tube in top thermocouple hole.
10. Check data acquisition computer for function
11. Adjust weighs to either 95 or 48 lbs as necassary.

INSTALLATION

Sample Prep

1. Build three 30 gauge type K thermocouples with four ceramic insulators.
2. Build one 24 gauge type K thermocouple with four ceramic insulators for Zone 1 temperature control.

3. Check calibration on all thermocouples.
4. Install the three thermocouples on the samples as shown in the figure with stainless steel bailing wire.
5. Install samples/thermocouples into creep testing fixture as per the figure. Without preloading the tightening bolts. See Figure.

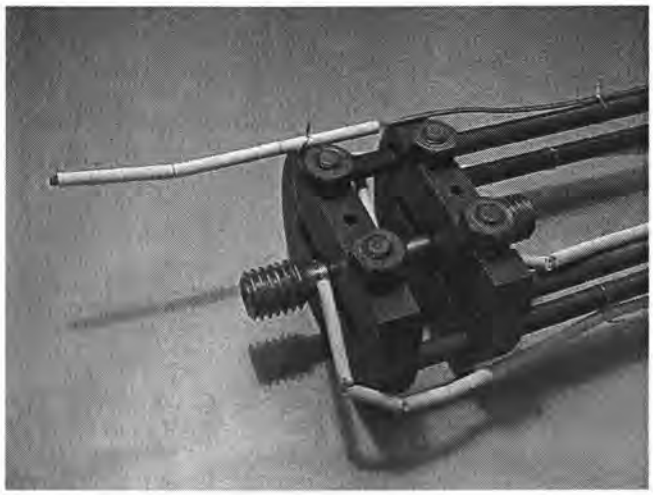

Figure 1. Installed Satec Sample.

6. Adjust thermocouples wires so they lead down the testing fixture supports.
7. Tie thermcouple wires to testing fixture with cadnium wire, to ensure intimate contact of T/C bead with sample.
8. Tie Zone 1 oven themocouple to the testing fixture such that its position during testing will rest in the top oven Zone 1.
9. Carefully tighten the fixture bolts keeping the sample perpendicular to the grip platforms. See Figure.

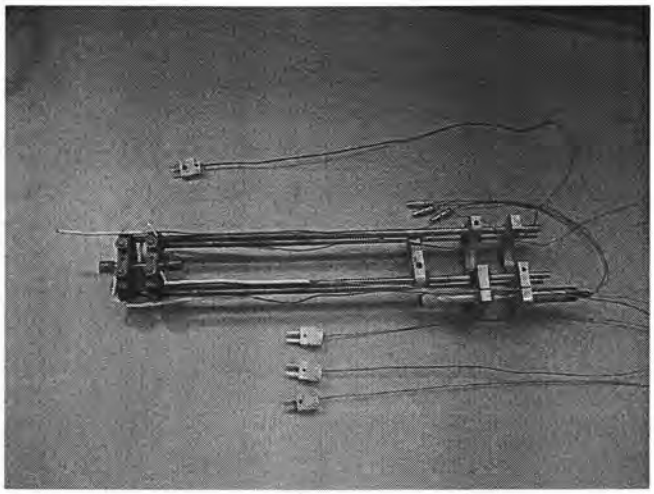

Figure 2. Complete Satec Testing Fixture.

SAMPLE INSTALLATION

1. Screw sample into top u-joint.
2. Screw bottom u-joint onto sample.
3. Add bottom Inconel rods to the load train.
4. Cut and install Ti getters, to aid in oxygen absorption. See Figure.

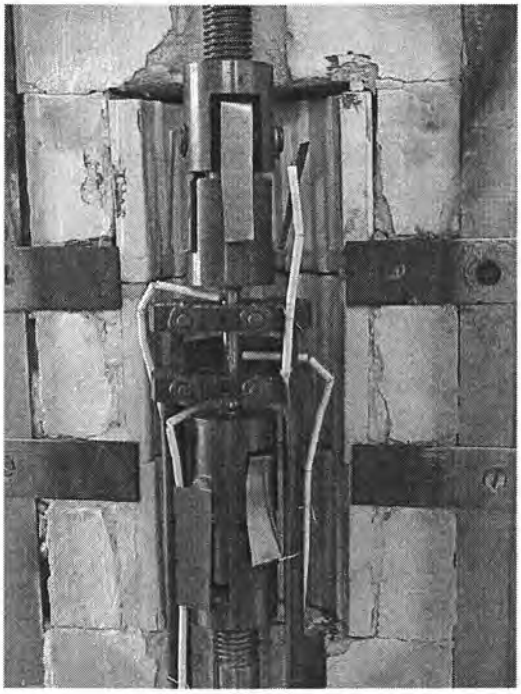

Figure 3. Installed Satec Sample With Getters.

5. Close oven door.
6. Connect sample thermocouples to Fluke Data Acquisition system. Top, middle and bottom thermocouples to channels 4, 5, and 6.
7. Install LVT into testing fixture.
8. Connect LVT red, blue and wires to the LVT amplifier.
9. Connect LVT amplifier coax cable to channel 3 in Fluke Data Unit.
10. Turn on amplifier change displacement selection on LVT amplifier to 0.5" setting.
11. Adjust micrometer on testing fixture such that the voltage read out is -3.000

TESTING CONDITIONS PREPARATION

1. Turn on Macintosh SE computer.
2. Load LabView file Tempmeasure2.lab.
3. Turn on Fluke Unit.
4. Turn on argon supply to 30 cfm.
5. Wait 15 minutes.
6. Turn on ovens to 550°C. Use slow ramping to testing temperature to avoid overshoot.
7. Adjust oven controllers so the sample temperature will be 550°C uniformly.

SAMPLE TESTING

1. Check weights.
2. Check argon bottle pressures to ensure adequate supply
3. Set argon flow rates to 30 cfm.
4. Load quenching syringe with distilled water.
5. Start Labview acquisition program.
6. Set wait time step to zero.
7. Record time.
8. Set creep tester switch to Auto.
9. Remove weights as neceassary to keep stress constant.
10. Record time after each weight removal.

11. On low stress tests after some strain set wait time step to 250.
12. Monitor creep rates.
13. When desired strain is reached or when sample fractures quench.(see additional procedures)
14. Continue cooling samples until cool enough to handle
15. When cool, carefully remove sample.
16. Remove remaining equipment and clean up machine.

QUENCHING PROCEDURES

1. Load syringe full of water.
2. Use gloves and safety glasses.
3. Hold oven bracket in right hand shut and undo latches with left.
4. Still keeping oven closed prepare syringe in left hand.
5. With left hand change switch settings to Manual and Up positions.
6. As soon as the load is off the sample open oven door and quench sample.
7. Change function switch to nuetral poistion.
8. Continue cooling sample
9. Turn off oven controllers and LVT amplifier.
10. Continue cooling sample
11. Remove LVT and disassemble LVT and connectors for open air drying
12. Continue cooling sample

REFERENCES

1. J. Sutliff, Lehigh University, Bethlehem, PA, May 1990.
2. P.B. Hirsch, A. Howie, R.B. Nicholson, and D.W. Pashley, "Electron Microscopy of Thin Crystals", Butterworths, 1965, p.422.

APPENDIX B

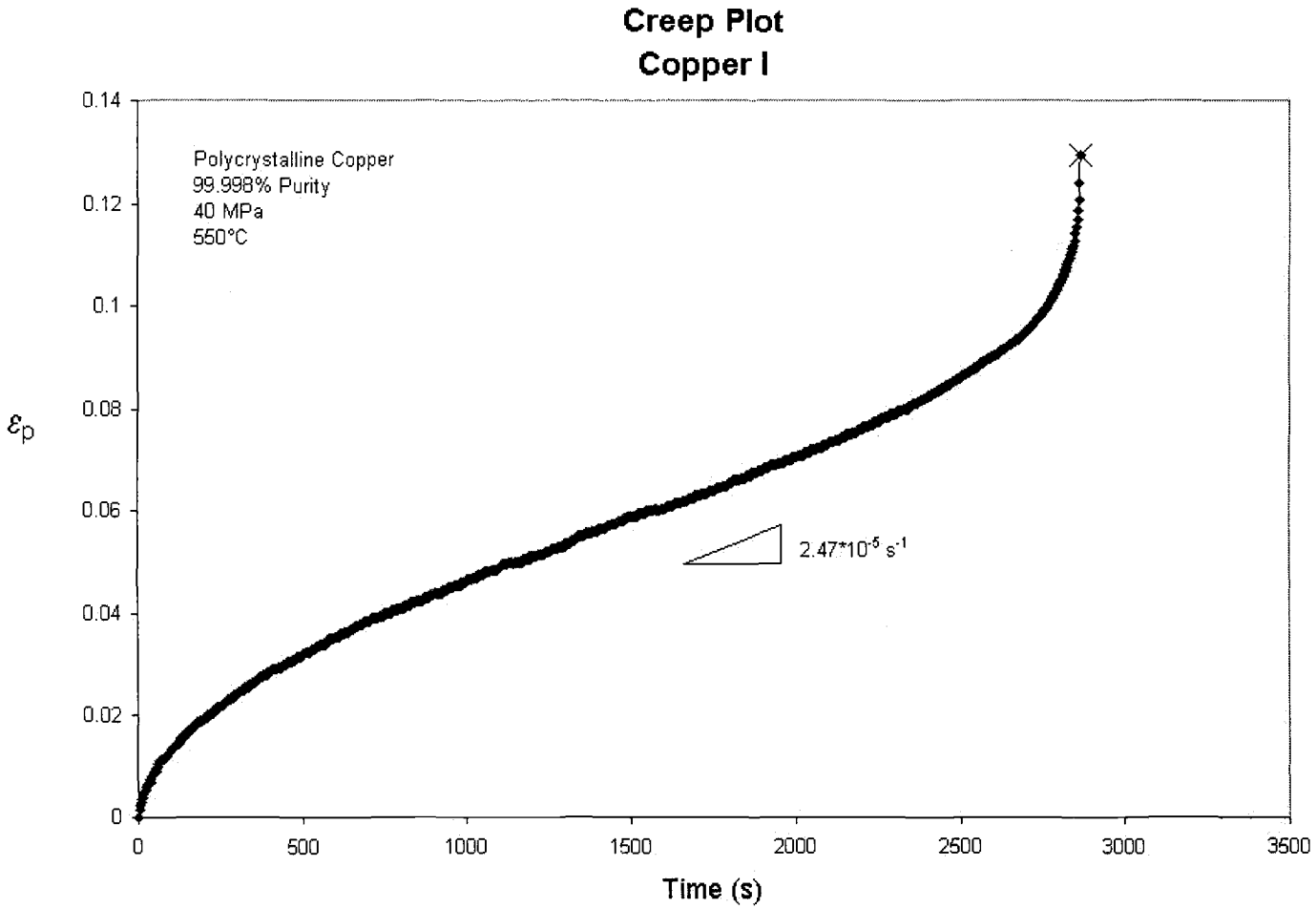

Figure 4. Creep Test of Copper I.

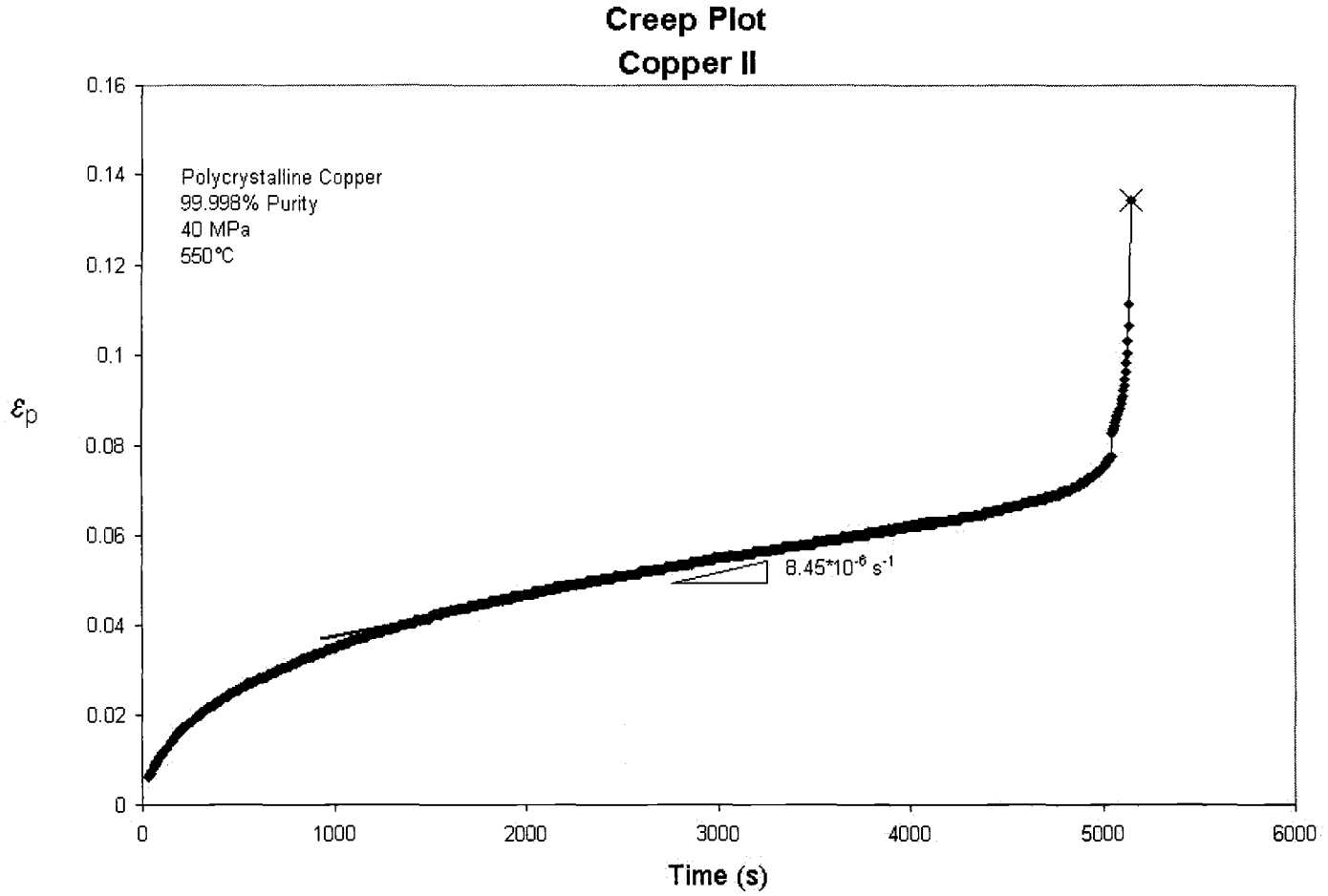

Figure 5. Creep Test of Copper II.

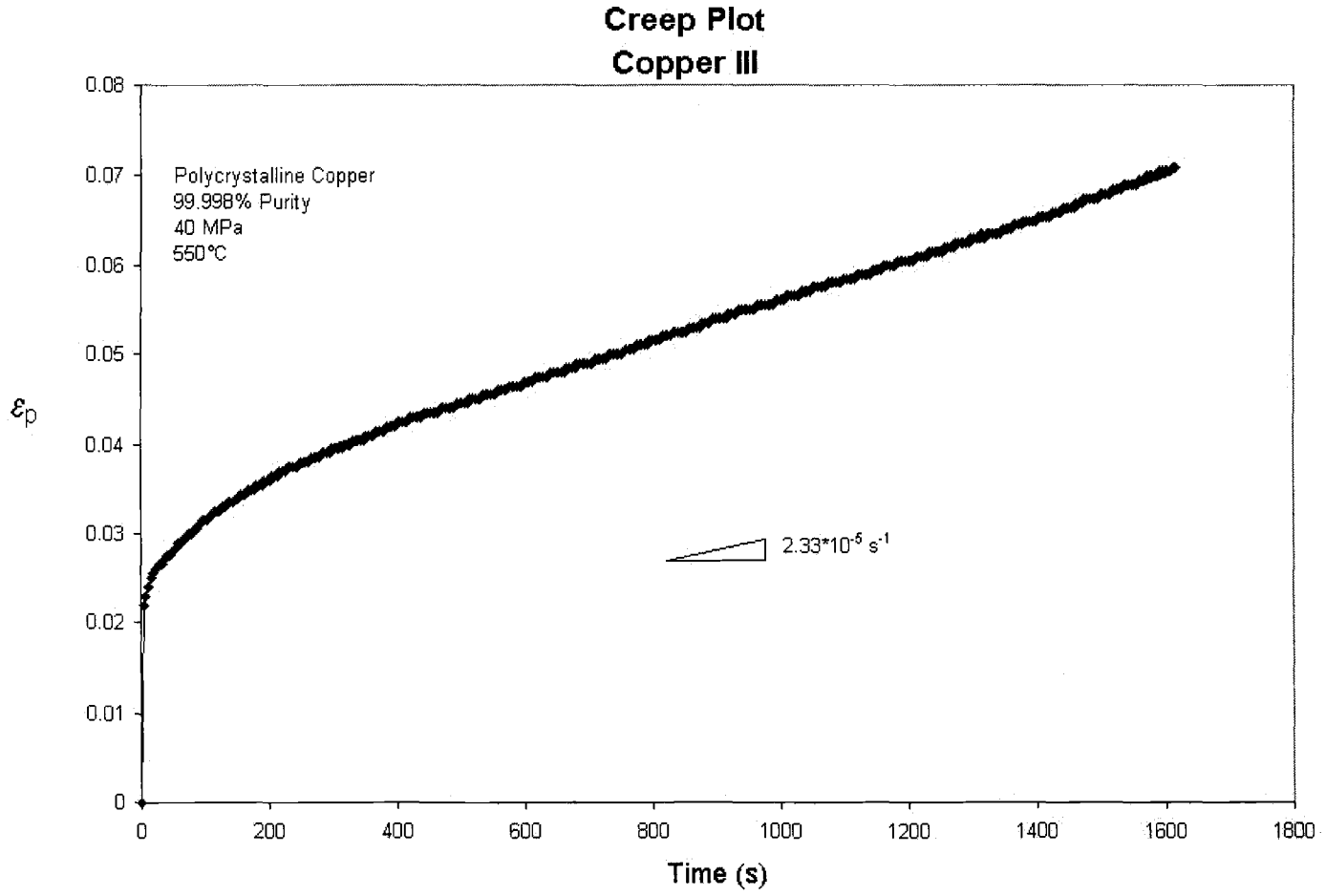

Figure 6. Creep Test of Copper III.

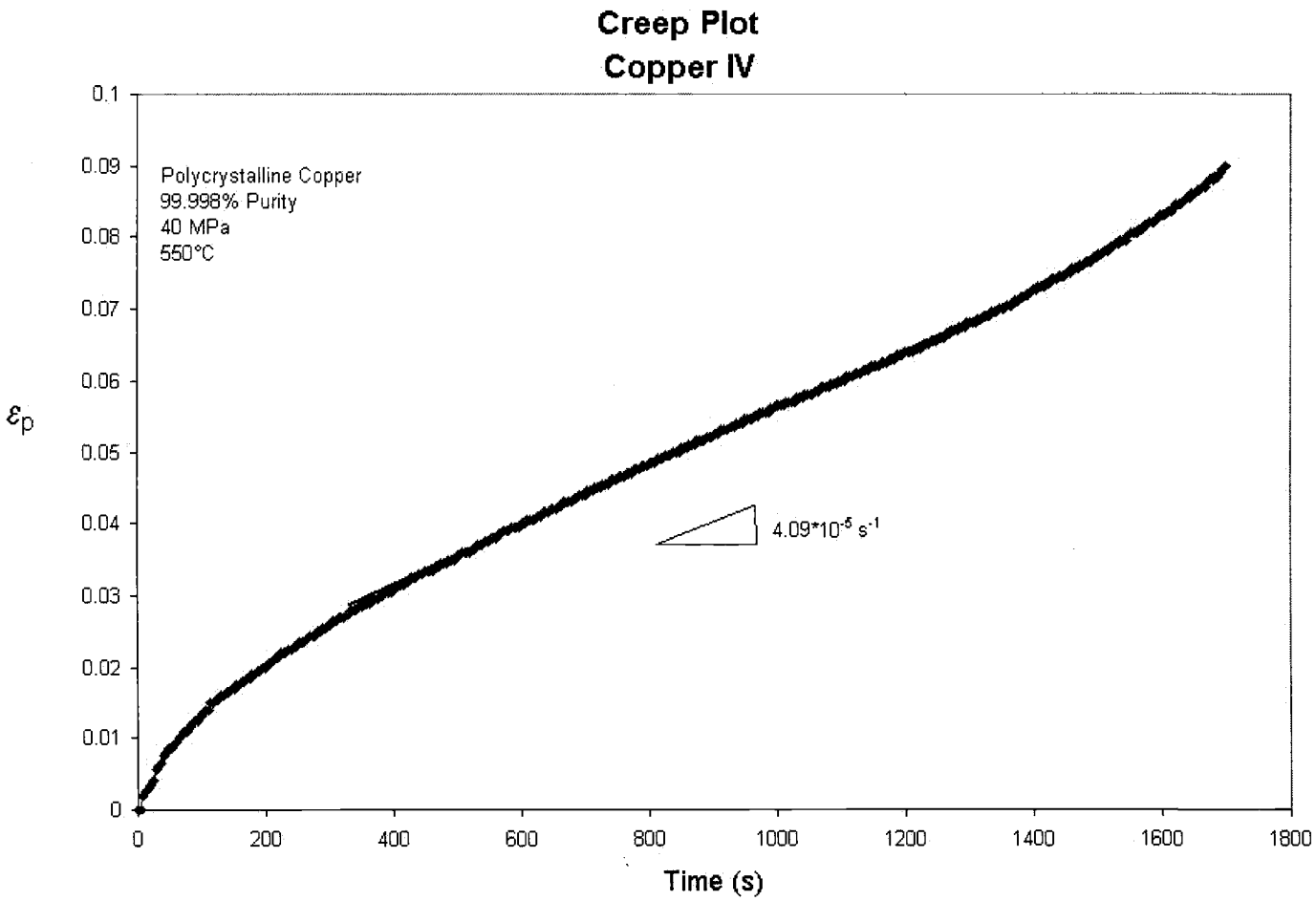

Figure 7. Creep Test of Copper IV.

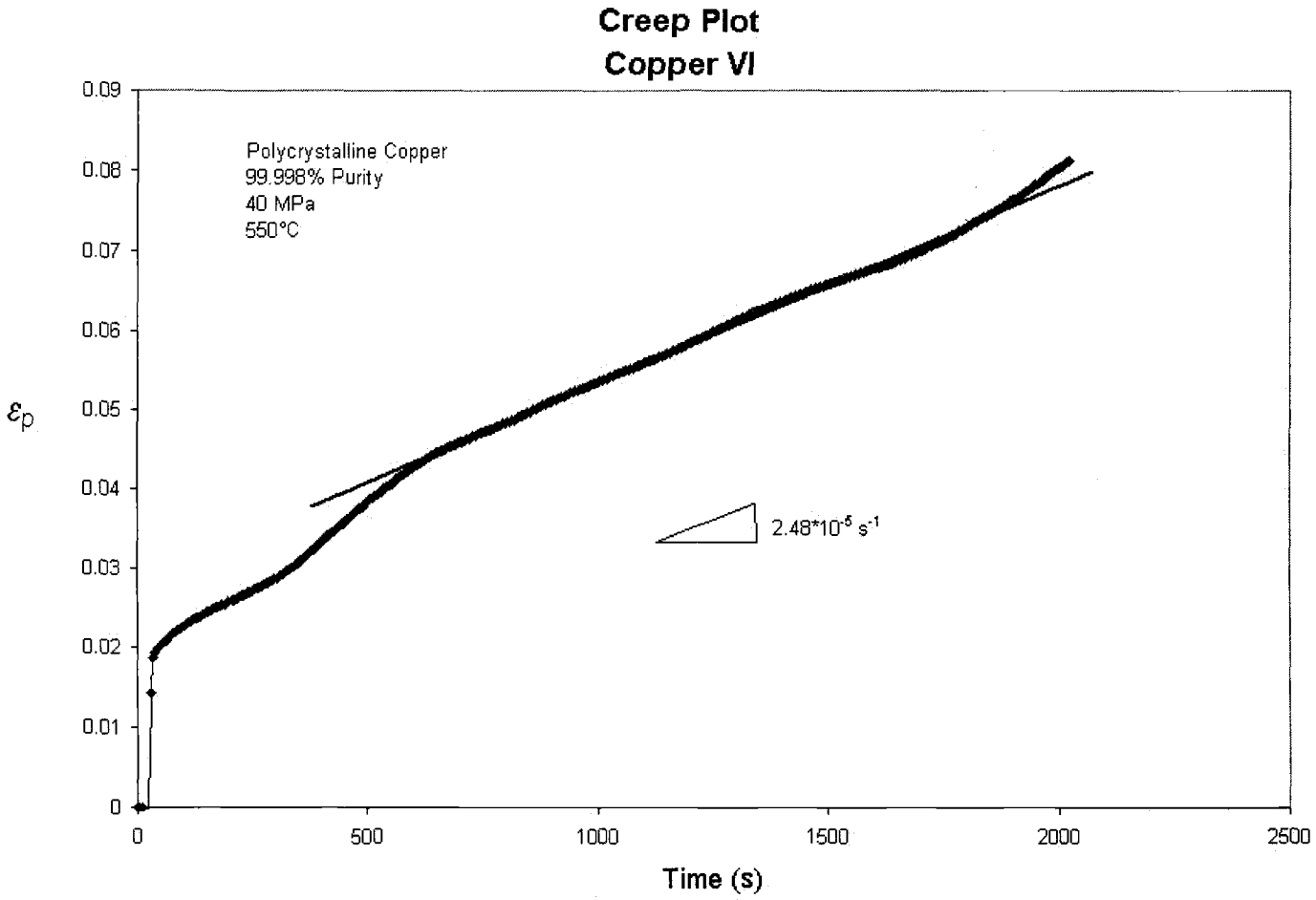

Figure 8. Creep Test of Copper VI.

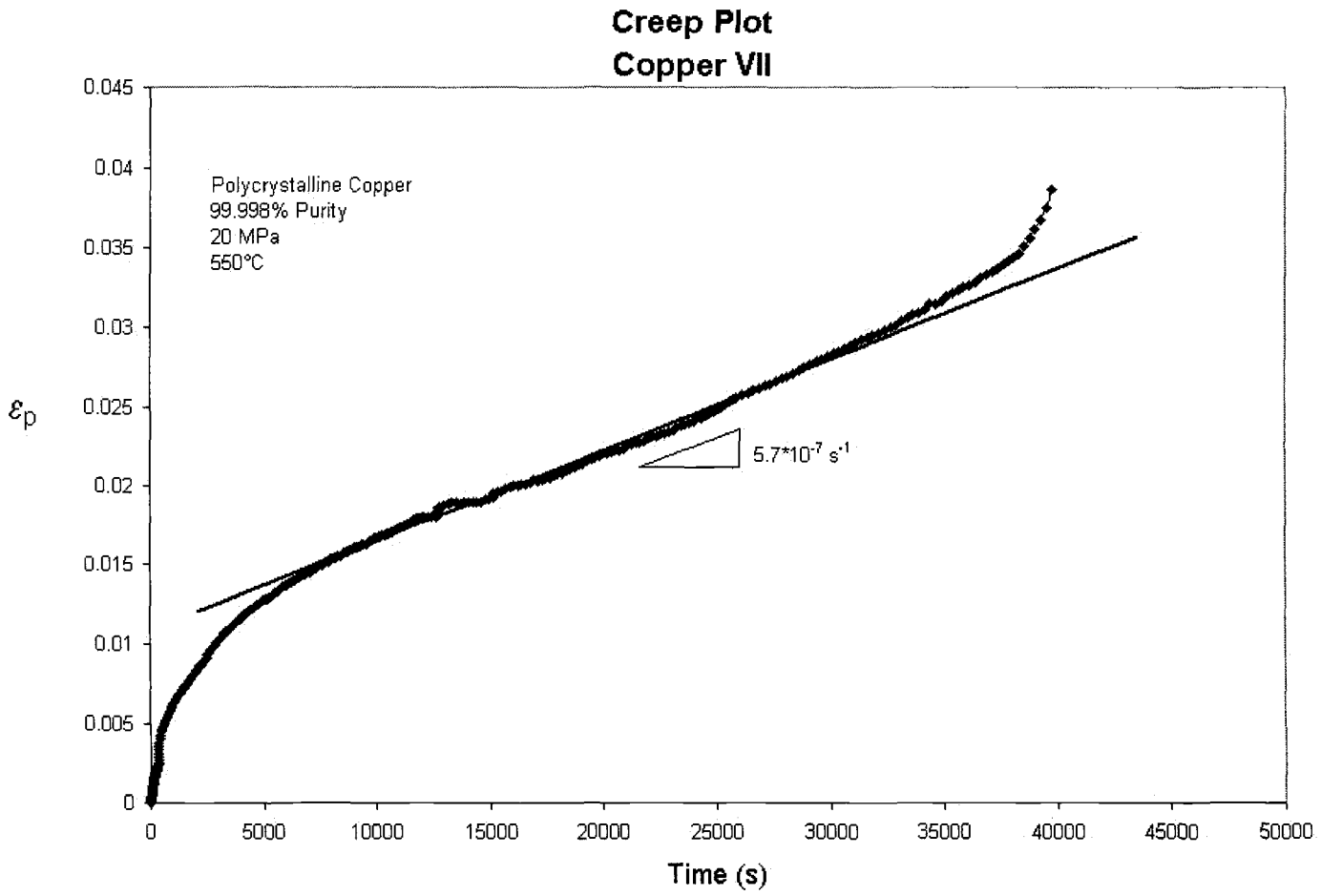

Figure 9. Creep Test of Copper VII.

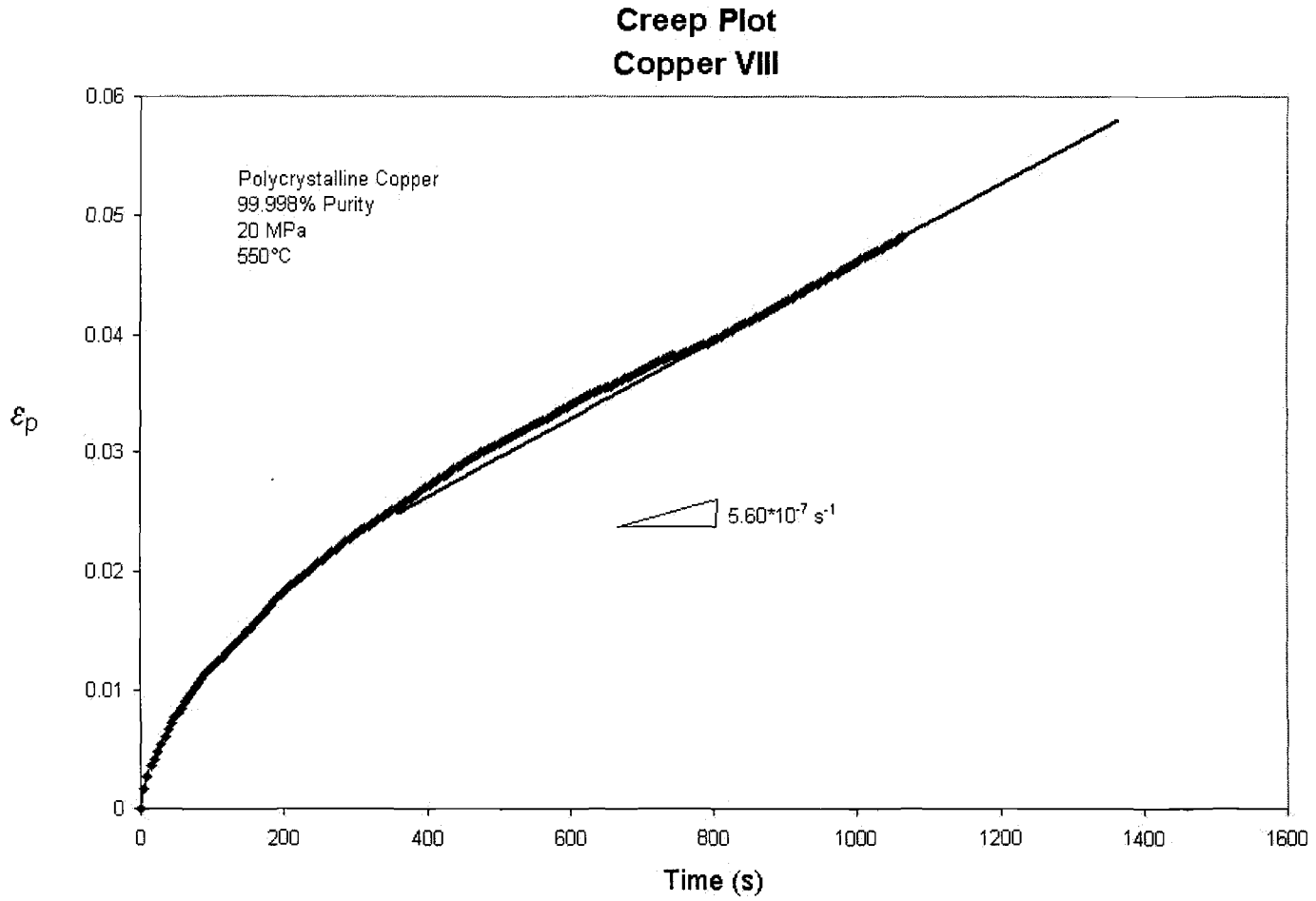

Figure 10. Creep Test of Copper VIII.

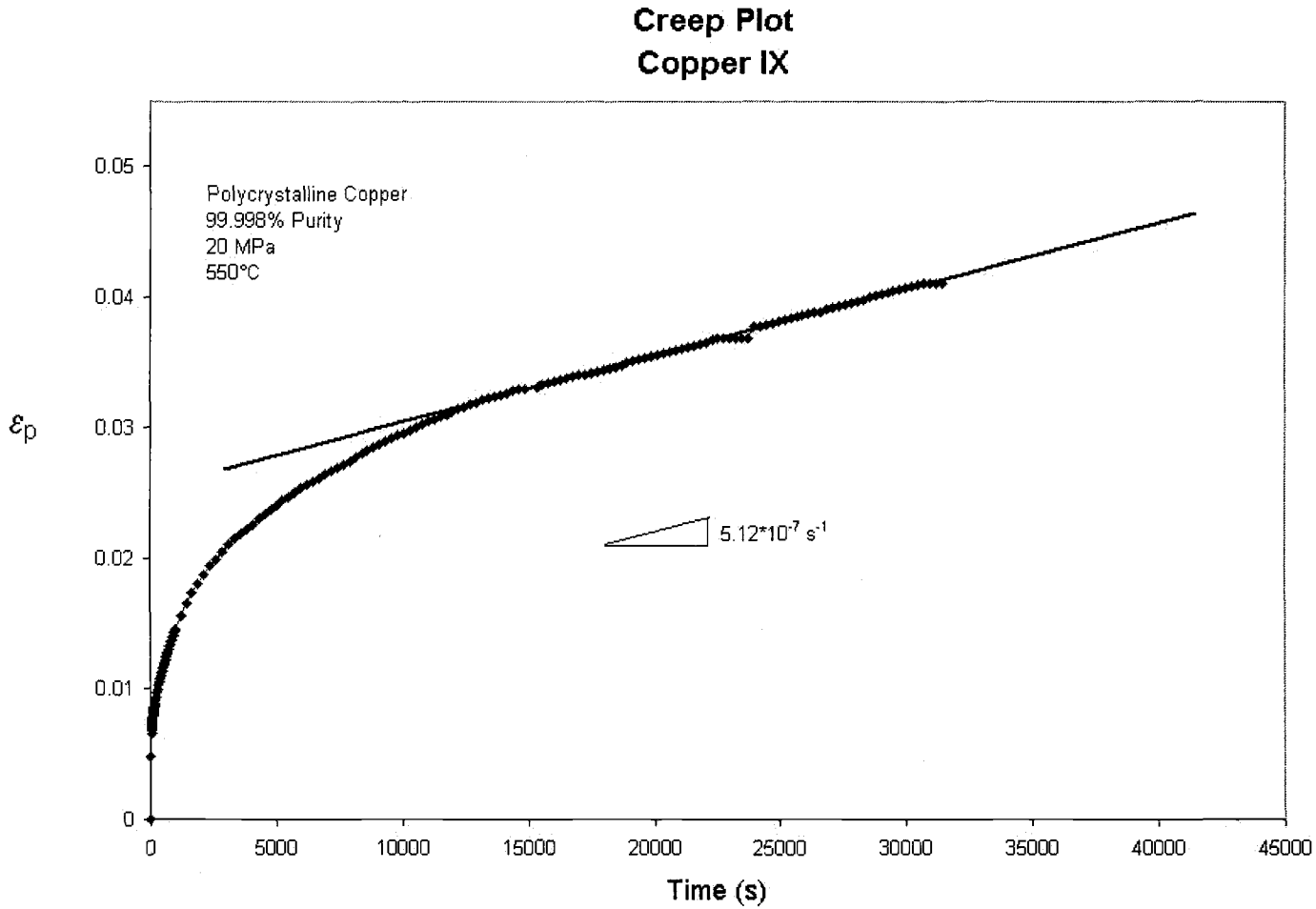

Figure 11. Creep Test of Copper IX.

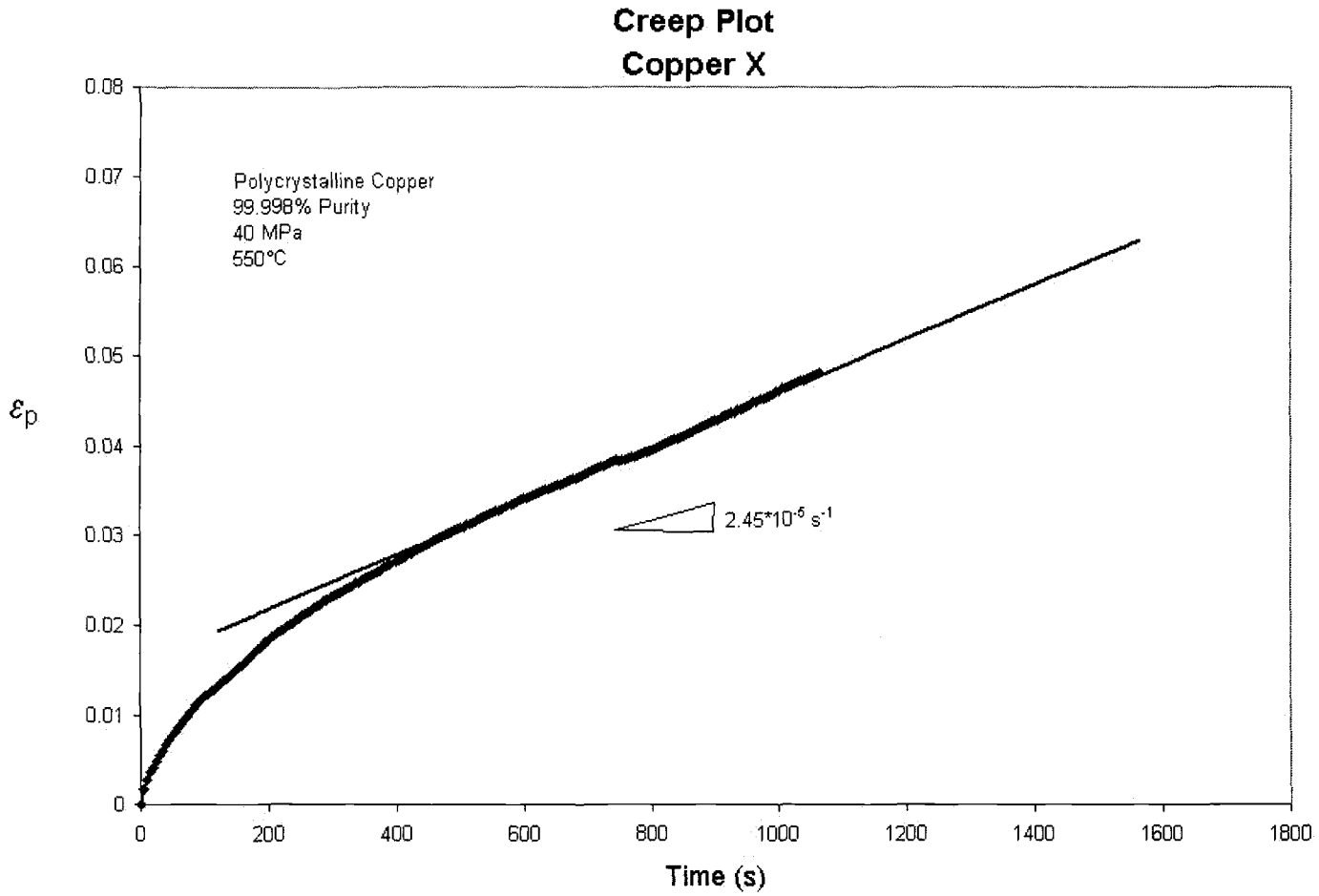

Figure 12. Creep Test of Copper X.